TAMPERE UNIVERSITY OF TECHNOLOGY

SAEED AFRASIABI GORGANI

PEAK POWER REDUCTION IN MULTICARRIER WAVEFORMS

Master of Science Thesis

Examiner:
Professor Dr. Tech. Markku Renfors
Examiners and topic approved in the
Faculty of Computing and Electrical
Engineering Council meeting on
September 2013

ABSTRACT

TAMPERE UNIVERSITY OF TECHNOLOGY
Master's Degree Programme in Information Technology
AFRASIABI GORGANI, SAEED : PEAK POWER REDUCTION IN MULTI-CARRIER WAVEFORMS
Master of Science Thesis, 77 pages, 0 Appendix pages
May 2014
Major: Communications Engineering
Examiner: Prof. Markku Renfors
Keywords: OFDM, OFDM/OQAM, FBMC, PAPR reduction, interpolation, SLM, PTS

Modern wireless communication systems employ multicarrier waveforms, such as the widely-used Orthogonal Frequency Division Multiplexing (OFDM) and the recent OFDM with Offset-QAM (OFDM/OQAM) schemes. An inherent characteristic of these waveforms is the high Peak-to-Average Power Ratio (PAPR). One of the last stages of the transmitter is the power amplifier, which needs specific attention as a major source of power consumption. For acceptable levels of power efficiency, the high PAPR issue causes distortion to the signal due to the nonlinearity of the power amplifier. This is a major drawback of multicarrier systems and, if not addressed properly, could overcome their advantages.

The PAPR reduction has been a topic of research for many years. By introduction of the new generations of the wireless systems, and perseverance of the more complicated multicarrier waveforms in finding their way into the proposed enabling technologies, this problem has gained interest again. Despite the relatively long history of research and the huge available literature, the problem is, to a great extent, still open. Among the disadvantages of the previously suggested PAPR reduction techniques, high computational complexity and complicated adaptation to the schemes such as OFDM/OQAM are standing out.

In this thesis, in addition to an in-depth review of the multicarrier waveforms in question, the two aforementioned issues are tackled. The challenges in adaptation of the PTS technique to the OFDM/OQAM are investigated. Concerning the general issue of high computational complexity, the feasibility of using interpolation instead of direct oversampling in PAPR measurement is studied. Depending on the bandwidth configuration, the interpolation could be remarkably beneficial.

PREFACE

As it has never happened so far, it is very unlikely that there will be a monograph published by me in the coming 4-5 years. I guess the first to come will be my PhD dissertation, which is again of the same nature as this piece of writing. Thus I can feel some excitement in finalizing this work and writing a preface to it. As the only careful reader of this manuscript is almost certainly my own self, I am targeting the future me in this preface.

Except for a good portion of Chapter 2 and few paragraphs from Chapters 3 and 5, this thesis is far behind my own expectations, not mentioning that it took more than a year. It's how I've always been. I've never finished any piece of my education in time and with good grades or with distinction or with Honors or whatever fancy label they might use for it. I've never really cared. This time I am a bit upset because I could have done a better and more organized research work. There were ideas, I had the motivation, a relaxed atmosphere, an impressively kind supervisor, but I didn't.

There are two things I have learned during this period of being in the research community, which I appreciate most. There might be more but I don't remember. Firstly, I learned that it is not easy at all, and very unlikely, to create a perfect piece of work. In addition, there are probably infinitely many states of human conditions which you can't account for. So passing judgment on others' work as well as developing self-expectations, though both essential in my opinion, must be done with great care.

The second thing is that, in our field, there are very few good researchers and very few good publications. In fact, being good is not appreciated that much. The basic feature of being good in my point of view is the quality that you know what you are doing down to a feasibly deep level. What I see out there is a huge business; the cycles of getting the grant, publishing more and more, and applying for further grants. My target at the moment is to be in that super-top tier, where only good work is done. It is very difficult and the chances are that it is a wrong goal, from a broader life prospective. We'll see.

And finally with the acknowledgments, as mentioned before, I've had a great supervisor, Professor Markku Renfors. His attitude toward many things has taught me a lot. I've had many good friends. I very much appreciate the synergism that I find in my friendship with Erfan Zamanian Dolati. I've had the great company of a very dear friend Azin Akbari. Erfan and Azin are among the extremely few sources of courage I may find in my way of life. I've had a very helpful and supporting circle of friends in Tampere: Farid, Kamiar, Mona, Nader, Orod, Peyman, Vida and my flatmate Miri. My roommates in the university, Alaa-Eddin and Sener, are the

two constant figures I've seen everyday and are good friends of mine. And finally I deeply, and too much briefly indeed, appreciate the support of my family members, my parents Akbar Afrasiabi Gorgani and Ziba Hoseyni Khayat, my brother Ali and my sister Sara.

Saeed Afrasiabi Gorgani
April 15, 2014
Berlin

CONTENTS

LIST OF FIGURES

LIST OF TABLES

LIST OF ACRONYMS

AFB	Analysis Filter Bank
CCDF	Complementary Cumulative Density Function
CMT	Cosine Modulated Multitone
CP	Cyclic Prefix
DFT	Discrete Fourier Transform
FFT	Fast Fourier Transform
ICI	Inter-Carrier Interference
ISI	Inter-Symbol Interference
OFDM	Orthogonal Frequency Division Multiplexing
OQAM	Offset QAM
PAPR	Peak-to-Average Power Ratio
PSD	Power Spectral Density
PTS	Partial Transmit Sequence
QAM	Quadrature Amplitude Modulation
SER	Symbol Error Rate
SFB	Synthesis Filter Bank
SLM	Selected Mapping
SMT	Staggered Modulated Multitone
TI	Tone Injection
TR	Tone Reservation
VSB	Vestigial Side-Band

1. INTRODUCTION

The mobile phone is the primary way of communication among individuals around the world. In some countries, they are completely replacing the landline telephone networks, leaving them behind as the emergency infrastructures. In addition, the application of these systems is much more than the voice communications. Nowadays, impressively high data-rate access to the Internet is available on the mobile phones and the demand for a higher rate is increasing constantly. Therefore, the research on the enabling technologies for the physical layer of the wireless communication systems has been and will be very active.

The recent generations of the cellular networks use the so-called multicarrier modulation, for instance the Orthogonal Frequency Division Multiplexing (OFDM). As the demand for data rate goes higher, the bandwidth assigned to the network increases as well, in addition to many other enhancements. The higher bandwidth causes the signal to experience a higher frequency selectivity from the channel side. Consequently, the compensation for the distortion done on the signal, namely the channel equalization, becomes more complicated in the receiver side. The key feature of the OFDM and similar multicarrier modulations is that they make the channel equalization significantly simpler.

As numerous wireless systems with different standards are working simultaneously, using high bandwidths, a set of new problems has emerged. Most importantly, with the current technology, unused bands in the spectrum are becoming scarce. Therefore, it is necessary to use the available spectrum more efficiently. One aspect of the solution is to design systems that coexist by being closely located in the spectrum. This is where the celebrated OFDM becomes disappointing, as it requires wide guard bands to avoid interference to the neighboring channels. Putting different signals tightly in adjacent channels requires waveforms which are better localized in the frequency domain.

Thanks to the advances in digital signal processing and the development of useful tools in the theory of filter banks, an old idea proposed in the 60's has attracted considerable attention recently. The modern name of this modulation scheme is "OFDM with offset QAM" or OFDM/OQAM. This scheme allows the use of customized pulse shapes, namely the prototype filter. In other words, by suitable choice of the pulse shape, the waveform can be made well-localized in the frequency do-

main. Although this scheme requires more computational complexity compared to the OFDM, it is a candidate for the next generations of wireless systems.

However, there is a major drawback with both of these schemes. The multicarrier nature of these waveforms causes the so-called high Peak-to-Average Power ratio (PAPR). In simple words, the multicarrier waveforms have very high fluctuations in the time domain, such that the signal has large peaks and steep valleys. The passband signal must be fed into a power amplifier before being transmitted through an antenna. Power amplifiers are nonlinear devices. The signal must be bounded to an interval of input power level where the device has linear behavior. Otherwise, it causes distortion.

Forcing either the power amplifier to have a wide linear range or the signal to fit into this range reduces the efficiency of the power amplifier. Apart from the energy saving aspect, it is clear that the power source is a major bottleneck in today's technology for portable devices that run on a battery. Therefore, it is necessary to reduce the PAPR of the waveforms in one way or another.

The PAPR reduction for OFDM signal has been an active area of research for the last 3 decades and numerous scientific papers have been published on the topic. One seemingly easy way to reduce the PAPR is to clip the signal deliberately and in a controlled manner. However, this method is not exactly as simple. It is shown that clipping the critically sampled signal is not helpful at all. Oversampling the signal before the clipping prevents the heavy distortion. However, this clipping causes out-of-band radiation which must be filtered. The filtering can be done by DFT-IDFT pairs, which causes some peak-regrowth. It is reported that clipping and filtering in several consecutive stages lead to acceptable PAPR reduction and performance. Therefore, the efficiency and feasibility of the method from the computational complexity point of view is not trivial.

There is a second category of the PAPR reduction methods which avoid any distortion. They are based on generating several representations of each OFDM symbol. Then the one with the least PAPR is chosen and transmitted. In the receiver the process must be reversed. These representations are generated based on some sort of known modification to the data symbols behind the OFDM symbol. In the Selected Mapping (SLM) technique and its more efficient successor Partial Transmit Sequences (PTS) technique, the phases of the data symbols are rotated. It is intuitively clear how this affects the PAPR, by considering that each data symbol modulates a complex exponential. They sum up constructively or destructively at different time instants. That is how the high time domain fluctuations happen. Therefore, it is expected that the "random" phase rotations of the data symbols change the PAPR, possibly to a lower value.

As explained, one stage of the algorithms used in the PAPR reduction techniques

is measuring the PAPR of the candidate sequences. The time-domain samples of the critically-sampled OFDM symbol do not have the resolution to capture the peaks of the symbol. The reliable measurement should be done with an oversampling of 4 or more. The oversampling is done, basically, by padding the data symbols with zeros, such that they fall near the ends of the spectrum, i.e., where the null subcarriers for the guard bands are located. Therefore, oversampling in its basic form requires a larger FFT size. It is possible to use interpolation to obtain the required oversampling, as will be studied.

One important difference between the OFDM and the OFDM/OQAM is that in OFDM, symbols are isolated in the time domain, i.e., they do not overlap. This makes everything easier when it comes to the iterative algorithms such as SLM or PTS. In the OFDM/OQAM, where the symbols are overlapping over several neighboring symbol, the situation is much more complicated. The PAPR must be measured over intervals of fixed length. In any interval, the time domain samples are a combination of several OFDM/OQAM symbols. In other words, reducing the PAPR of a segment of the overall signal needs joint modification of several symbols.

The present thesis is organized into four chapters. It begins with a detailed tutorial-style review of the main idea behind the offset-QAM scheme. Chapter 3 explains the high PAPR issue in the two multicarrier schemes: OFDM and OFDM/OQAM. Chapter 4 reviews an important category of techniques including the Selected Mapping (SLM) and the Partial Transmit Sequences (PTS) and discusses their adaptation to the OFDM/OQAM scheme. Finally, application of the interpolation, as a way of achieving oversampled signal in the PAPR reduction methods is investigated in Chapter 5.

2. MULTICARRIER WAVEFORMS

In this chapter, the multicarrier waveforms that are studied in this report are introduced. The intention is to develop the schemes in a tutorial fashion. In the first section, the general model for a multipulse modulation and its requirements are discussed. A multipulse modulation is a term referring to the general case where more than one pulse shape is used, of which the multicarrier modulation is a special case.

In the second section, the popular Orthogonal Frequency Division Multiplexing (OFDM) is explained. It is well-known that the OFDM lacks the features required for the emerging applications. This is mainly due to the rectangular pulse shape which slowly decays in the frequency domain. In the third section, it is shown that using other pulse shapes is not straightforward. In the fourth section, an old scheme from the 60s referred to as Cosine Modulated Multitone (CMT) is developed. Based on that, the fourth section explains the Staggered Modulated Multitone (SMT) scheme, which is the main objective of this chapter.

There has been the attempt to cover all the aspects required to understand the underlying principles of these schemes. In addition, the continuous-time models are emphasized, as the discrete-time development imposes extra complexity to the concepts. At the end, the discrete-time model and the pulse shape considerations are discussed briefly, in order to make the implementation aspect clear.

2.1 Multipulse modulation

Consider a multipulse modulation of the form

$$s(t) = \sum_{k=-\infty}^{+\infty} \sum_{n=0}^{N-1} A_{k,n} h_n(t - kT), \tag{2.1}$$

where $A_{k,n}$ is the data symbol that modulates the n^{th} subcarrier in the k^{th} symbol interval. The modulation structure is illustrated in Figure 2.1. In order to avoid Inter-Symbol Interference (ISI), the set of pulses $h_n(t)$ for $n = 0, \ldots, N-1$ must satisfy the ordinary Nyquist criterion

$$h_n(t) * h_n^*(-t)|_{t=kT} = \delta_k, \quad n = 0, \ldots, N-1, \tag{2.2}$$

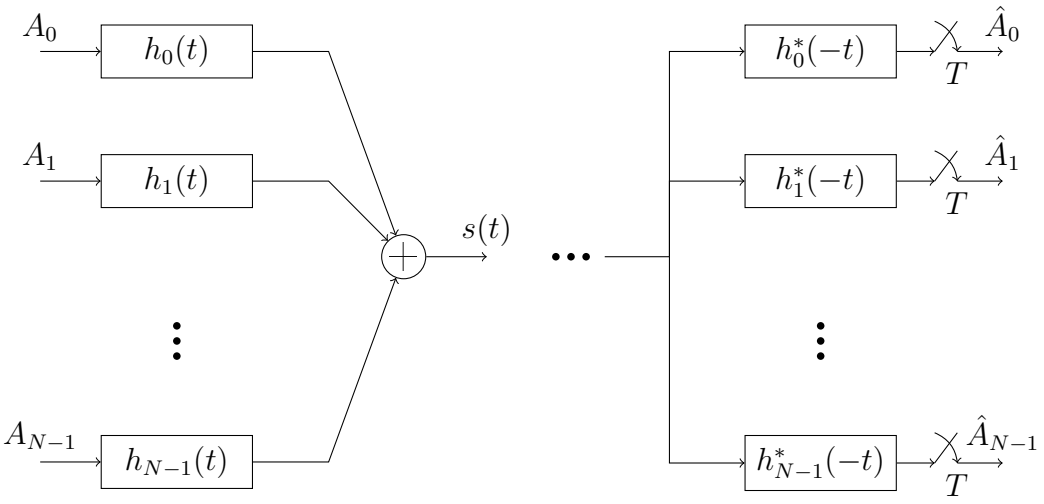

Figure 2.1: The general structure of the multipulse modulation.

where δ_k is the Kronecker delta function and is defined as

$$\delta_k = \begin{cases} 1, & k = 1 \\ 0, & k \neq 1. \end{cases} \tag{2.3}$$

Equation (2.2) is, in the frequency domain, equivalent to

$$\frac{1}{T} \sum_{m=-\infty}^{+\infty} |H_n(j(\omega + m\frac{2\pi}{T}))|^2 = 1, \quad n = 0, \ldots, N-1. \tag{2.4}$$

where $H_n(j\omega)$ is the Fourier transform of $h_n(t)$. In order to avoid Inter-Channel Interference (ICI), the chosen pulses must satisfy the generalized Nyquist criterion [13, p. 235]

$$h_n(t) * h_l^*(-t)|_{t=kT} = \delta_k \delta_{l-n}, \quad n, l = 0, \ldots, N-1, \tag{2.5}$$

or equivalently in the frequency domain

$$\frac{1}{T} \sum_{m=-\infty}^{+\infty} H_n(j(\omega + m\frac{2\pi}{T}))H_l^*(j(\omega + m\frac{2\pi}{T})) = \delta_{l-n}, \quad n, l = 0, \ldots, N-1. \tag{2.6}$$

It is clear that the ordinary Nyquist criterion is the special case of its generalized version for $n = l$.

A simple and straightforward way to design the pulses in (2.1) which satisfy the generalized Nyquist criterion is to isolate them in either the time or the frequency domain. The widely used OFDM scheme is based on isolation in the time domain, as will be explained in the next.

2.2 Isolation in time, OFDM

Time domain isolation is probably a natural choice. The rectangular pulse shape, and hence a sinc shape in the frequency domain, is a popular one. Such a pulse would then need infinite bandwidth as a sinc function is theoretically nonzero over $\mathbb{R}$. Therefore, the practical case is an approximation of such rectangular pulses. This scheme is referred to as the Orthogonal Frequency Division Multiplexing (OFDM). In the sequel, the OFDM signal model is described based on the notation commonly used in the literature.

The continuous-time baseband signal model for a single symbol of the OFDM is

$$s(t) = \frac{1}{\sqrt{N}} \sum_{k=0}^{N-1} X_k e^{j2\pi k f_\Delta t} \quad t \in [0, T], \tag{2.7}$$

where N is the number of subcarriers, the vector

$$\mathbf{X} = [X_0, X_1, \ldots, X_{N-1}]^T \tag{2.8}$$

denotes the data symbols, T is the OFDM symbol duration and

$$f_\Delta = \frac{1}{T} \tag{2.9}$$

is the frequency spacing of subcarriers. In this text, a data symbol is distinguished from an OFDM symbol explicitly unless it is clear from the context. Note that the pulses used in OFDM, according to (2.1), are

$$h_n(t) = \text{rect}(\frac{t - T/2}{T}) e^{j2\pi \frac{n}{T} t}, \quad n = 0, \ldots, N-1, \tag{2.10}$$

where

$$\text{rect}(t) = \begin{cases} 1 & |t| \leq \frac{1}{2} \\ 0 & \text{elsewhere.} \end{cases} \tag{2.11}$$

The critically-sampled discrete-time signal model is accordingly obtained as

$$s[k] = s(kT_s) = \frac{1}{\sqrt{N}} \sum_{n=0}^{N-1} X_n e^{j2\pi \frac{n}{T} k T_s}, \quad k = 0, 1, \ldots, N-1, \tag{2.12}$$

where the sampling frequency is $\frac{1}{T_s} = N f_\Delta$. Therefore, $s[k]$ can be written as

$$s[k] = \frac{1}{\sqrt{N}} \sum_{n=0}^{N-1} X_n e^{j \frac{2\pi}{N} nk}, \quad k = 0, 1, \ldots, N-1. \tag{2.13}$$

The scalar factor $\frac{1}{\sqrt{N}}$ is necessary to derive the statistical properties of the OFDM symbols, as will be shown in section 3.3.

It is interesting to observe that (2.13) is the expression for the Inverse Discrete Fourier Transform (IDFT). This makes it possible to use the very popular implementation of IDFT known as Fast Fourier Transform (FFT) to do the OFDM modulation. The scalar factor may vary among the different FFT implementations.

Channel equalization

The effect of a frequency-selective channel, caused by multipath propagation, on a signal can be modeled and illustrated by the effect of an FIR filter. The received signal is the sum of multiple replicas of the signal with different delays and attenuations. In other words, the symbols are mixed and the so-called Inter-Symbol Interference (ISI) happens. Thus the channel can be viewed as a filter in the transmitter-receiver chain, which is not taken into account when the pulse shape is designed. As a matter of fact, it is not possible to predict and account for the channel in advance. Therefore, the channel must be estimated and equalized. The problem is that equalizing a severely frequency-selective channel, which is the case in the modern applications, requires a high-order FIR filter. In addition, the equalization must be adaptive as the channel changes in time, which becomes more complex for such a filter.

The main motivation for using the multicarrier modulation, particularly the OFDM as a widely used technique, is to avoid the complex channel equalization required for the single-carrier schemes. This facility requires that the channel functions as a subcarrier-wise multiplication of the data symbols with complex gains [22]. In other words, it is necessary that the channel response is flat in each subcarrier bandwidth.

In the OFDM, each subcarrier is spread over the entire available bandwidth. It takes a distance of several subcarriers until the so-called sidelobes drop to a negligible level. However, as the OFDM symbols are isolated in the time-domain, it is possible to change the linear convolution of the channel to circular convolution and establish the subcarrier-wise multiplication of the frequency response of the channel with the data symbols. This is done by inserting a Cyclic Prefix (CP) to the beginning of the OFDM symbol [20, Chapter 8]. In the receiver side, the CP is discarded before the demodulation.

In the schemes developed in the following sections, the pulse shapes are well-localized in the frequency domain. If the bandwidth of the subchannels is relatively small and the number of them is high, then each of them experiences an approximately flat channel response [8].

2.3 Overlapping in time and frequency

A major drawback of the OFDM scheme is the heavy overlapping of the neighboring subchannels in the frequency domain. This drawback stands out most when it is desired to have the multicarrier system work in coexistence with other systems [24]. It is often necessary to have a spectrally well-contained waveform, a property that the OFDM waveform mainly lacks.

Here we investigate the problem from the viewpoint of the uniform framework explained before. It is clear that pulses with mild behavior in the time domain have better spectral containment. For simplicity, and to keep the discussion close to the well-known schemes, pulses are allowed to overlap over only the adjacent subchannels. This corresponds to a 100% or lower roll-off.

A first thought would suggest to modify the OFDM modulation only by changing the pulse shape from a rect(t/T) to a more well-behaved waveform $q(t)$, i.e.,

$$h_n(t) = q(t)e^{j\frac{2\pi}{T}nt}, \tag{2.14}$$

where $q(t)$ is the basic pulse shape designed for a symbol duration of T. The frequency transform of each pulse is

$$H_n(j\omega) = Q(j(\omega - n\frac{2\pi}{T})), \tag{2.15}$$

where $Q(j\omega)$ is the Fourier transform of $q(t)$. Applying the ordinary Nyquist criterion as in (2.4), $Q(j\omega)$ must satisfy

$$\frac{1}{T}\sum_{m=-\infty}^{+\infty} |Q(j(\omega - n\frac{2\pi}{T} + m\frac{2\pi}{T}))|^2 = 1, \tag{2.16}$$

which can be rewritten via a change of variable as

$$\frac{1}{T}\sum_{m=-\infty}^{+\infty} |Q(j(\omega - m\frac{2\pi}{T}))|^2 = 1. \tag{2.17}$$

This shows that $Q(j\omega)$ must be a Nyquist pulse, e.g., as the popular root-raised cosine pulse. Note that the ordinary Nyquist criterion restricts only the magnitude of $Q(j\omega)$.

Following the assumption that $Q(j\omega)$ overlaps only over the adjacent subchannels, as sketched in Figure 2.2, the generalized Nyquist criterion as in (2.6) can be simplified. It is clear that the criterion is satisfied for $l - n > 1$, as the more distant

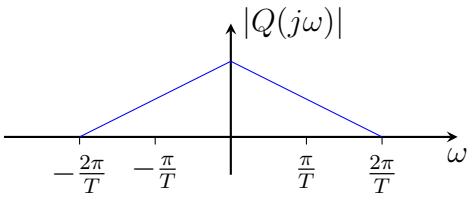

Figure 2.2: A sketch of the amplitude of the basic pulse shape in frequency domain, $Q(j\omega)$

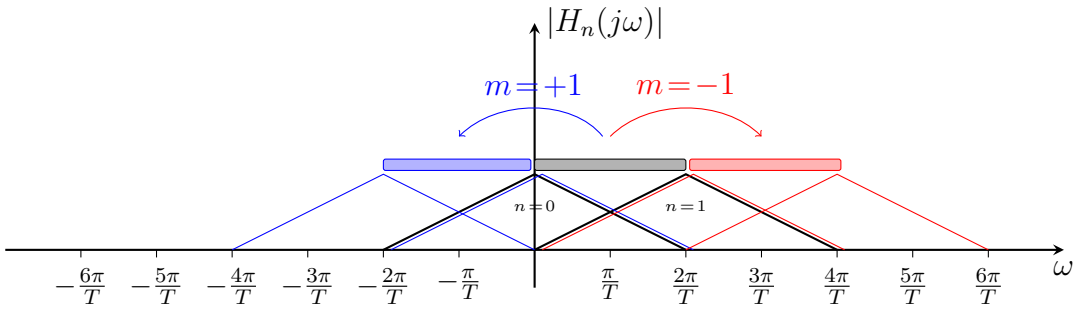

Figure 2.3: The construction of the expression in (2.19). A hashed area indicates the interval where a product is nonzero.

pulses never overlap theoretically. Hence,

$$\frac{1}{T}\sum_{m=-\infty}^{+\infty} H_n(j(\omega+m\frac{2\pi}{T}))H_{n+1}^*(j(\omega+m\frac{2\pi}{T}))=0 \tag{2.18}$$

must be met. In terms of $Q(j\omega)$, and after a change of variable, we have

$$\frac{1}{T}\sum_{m=-\infty}^{+\infty} Q(j(\omega+m\frac{2\pi}{T}))Q^*(j(\omega+(m-1)\frac{2\pi}{T}))=0. \tag{2.19}$$

Note that the choices of $l=n+1$ and $l=n-1$ are equivalent.

The expression in (2.19) is clearly periodic over intervals of $\frac{2\pi}{T}$. Therefore, we can investigate the interval of $\omega\in[-\frac{\pi}{T},\frac{\pi}{T}]$. Figure 2.3 reveals the contribution of each term to the summation in (2.19). The black curves refer to the adjacent pulses for $n=0$ and $n=1$. The shifted copies of the product of these pulses build the summation in (2.19). For simplicity, only the nonzero interval of the product is indicated by a gray hashed box. Focusing on $\omega\in[-\frac{\pi}{T},\frac{\pi}{T}]$, the figure shows all the terms which contribute and their nonzero intervals.

Therefore, it is clear from Figure 2.3 that the summation in the desired interval can be simplified to

$$Q(j\omega)Q^*(j(\omega-\frac{2\pi}{T}))+Q(j(\omega+\frac{2\pi}{T}))Q^*(j\omega)=0,\quad \omega\in[-\frac{\pi}{T},\frac{\pi}{T}], \tag{2.20}$$

which includes the terms corresponding to $m = 0$ and $m = 1$. Furthermore, Figure 2.3 shows that the nonzero intervals of the products in (2.19) do not overlap. In other words, both of the terms in (2.20) must be zero. Furthermore, since they differ only by a frequency shift, the generalized Nyquist criterion finally reduces to

$$Q(j\omega)Q^*(j(\omega - \frac{2\pi}{T})) = 0, \quad \omega \in [-\frac{\pi}{T}, \frac{\pi}{T}]. \tag{2.21}$$

It is clear that generally for a complex number a, $|a|e^{j\theta_a} = 0$ if and only if $|a| = 0$. Thus $|Q(j\omega)|$ cannot lead to (2.21) as it would be absurd. Therefore, it is not possible to satisfy the generalized Nyquist criterion by these pulses. In other words, following the general idea of the OFDM and changing the pulse shapes does not lead to a working scheme.

2.4 Cosine Modulated Multitone (CMT)

There is a working modulation scheme first developed by Chang [5], which is the basis for the so-called Cosine Modulated Multitone (CMT) scheme. The pulses $h_n(t)$, as in (2.1), are defined as

$$h_n(t) = q(t)\cos\left((n + \frac{1}{2})\frac{\pi}{T}t\right), \quad n = 0, 1, \ldots, N-1, \tag{2.22}$$

where $q(t)$ is a Nyquist pulse for a symbol duration of $2T$. In the frequency domain, they are

$$H_n(j\omega) = \frac{1}{2}\left[Q(j(\omega + \frac{\pi}{2T} + n\frac{\pi}{T})) + Q(j(\omega - \frac{\pi}{2T} - n\frac{\pi}{T}))\right], \quad n = 0, 1, \ldots, N-1. \tag{2.23}$$

Figure 2.4 illustrates the arrangement of the pulses in the frequency domain. The minimum bandwidth required for $q(t)$ is $\frac{\pi}{T}$. Repeating the assumption of 100% roll-off, it needs twice the minimum bandwidth, $\frac{2\pi}{T}$. Thus the frequency separation is $\frac{\pi}{T}$. However, the key difference here is that the pulses are real and double-sided in frequency. If real data symbols are used, the symmetry of the pulses allows the application of the Vestigial Side Band (VSB) modulation.

It is clear from Figure 2.4 that $h_n(t), n = 1, 2, \ldots, N$ satisfies the ordinary Nyquist criterion for the symbol duration T provided that $q(t)$ does so for $2T$. Here the role of the extra frequency shift by $\frac{\pi}{2T}$ and then the modulation to $-\frac{n\pi}{T}$ and $\frac{n\pi}{T}$ becomes clear.

The ordinary Nyquist criterion sets constraints on $A(\omega) = |Q(j\omega)|$. Applying the generalized criterion will then reveal the requirement for the phase response $\theta(\omega) = \arg\, Q(j\omega)$ as will be explained shortly. Since the pulses overlap only over the adjacent ones, then it is enough to consider the cases $l = n + 1$ or $l = n - 1$. It

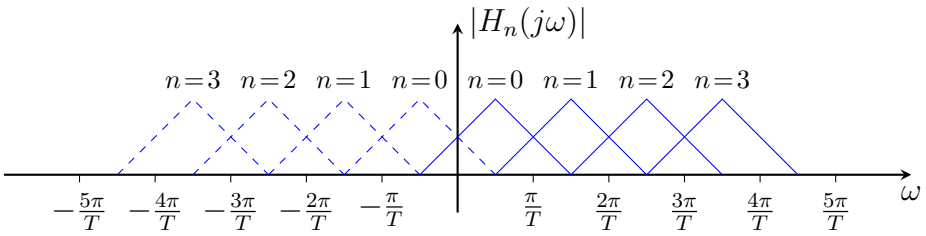

Figure 2.4: A frequency domain illustration of the pulses in the CMT scheme. The dashed curves indicate the negative frequency part of the double-sided pulses.

is clear from (2.6) that these two cases are equivalent. Rewriting (2.6) for $l = n+1$, we have

$$\frac{1}{T}\sum_{m=-\infty}^{+\infty} H_n(j(\omega + m\frac{2\pi}{T}))H_{n+1}^*(j(\omega + m\frac{2\pi}{T})) = 0. \tag{2.24}$$

Substituting (2.23) and after some manipulation, it follows as

$$\begin{aligned}\frac{1}{T}\sum_{m=-\infty}^{+\infty} &[Q(j(\omega - (2n+1)\frac{\pi}{2T} + m\frac{2\pi}{T})) + Q(j(\omega + (2n+1)\frac{\pi}{2T} + m\frac{2\pi}{T}))]\times \\ &[Q^*(j(\omega - (2n+3)\frac{\pi}{2T} + m\frac{2\pi}{T})) + Q^*(j(\omega + (2n+3)\frac{\pi}{2T} + m\frac{2\pi}{T}))] = 0.\end{aligned} \tag{2.25}$$

Two of the four product terms vanish as they do not overlap. Therefore, we have

$$\begin{aligned}\frac{1}{T}\sum_{m=-\infty}^{+\infty} &Q(j(\omega - (2n+1)\frac{\pi}{2T} + m\frac{2\pi}{T}))Q^*(j(\omega - (2n+3)\frac{\pi}{2T} + m\frac{2\pi}{T})) + \\ &Q(j(\omega + (2n+1)\frac{\pi}{2T} + m\frac{2\pi}{T}))Q^*(j(\omega + (2n+3)\frac{\pi}{2T} + m\frac{2\pi}{T})) = 0.\end{aligned} \tag{2.26}$$

Since this expression is 2π-periodic, its evaluation can be made easier by inspecting it over only $\omega \in [-\frac{\pi}{T}, \frac{\pi}{T}]$.

The procedure to derive (2.26) is visualized in Figure 2.5a for $n = 1$ and in Figure 2.5b for $n = 0$. Here we proceed with the case of $n = 1$, as an example. It is clear that in (2.26) the terms referring to $m = 1$ and $m = -1$ partly fall into the interval of $\omega \in [-\frac{\pi}{T}, \frac{\pi}{T}]$. Therefore, removing the remaining frequency shifts that fall outside the interval, we have

$$Q(j(\omega - \frac{\pi}{2T}))Q^*(j(\omega + \frac{\pi}{2T})) + Q(j(\omega + \frac{\pi}{2T}))Q^*(j(\omega - \frac{\pi}{2T})) = 0, \tag{2.27}$$

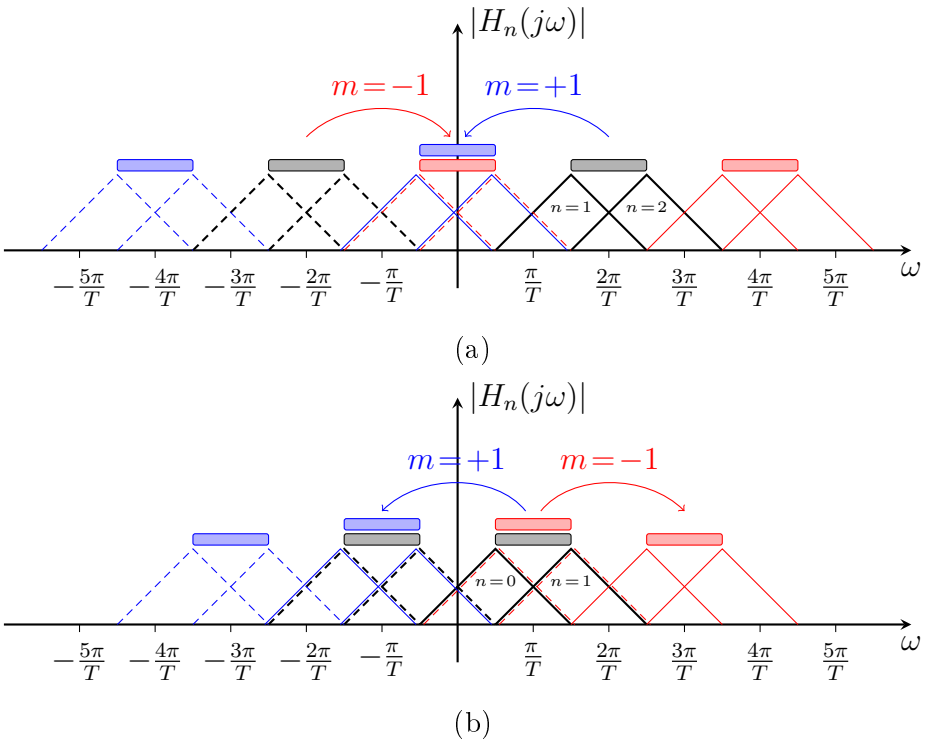

Figure 2.5: Illustration of the procedure taken to reach at (2.26) for (a) $n = 1$ and (b) $n = 0$. The blue, red and black components indicate the $m = 1$, $m = -1$ and $m = 0$ terms, respectively. Dashed lines show the negative frequency part of the pulses. The hashed areas indicate nonzero intervals.

which is, since $\alpha + \alpha^* = 2\mathrm{Re}\{\alpha\}$, equivalent to

$$2\mathrm{Re}\left\{Q(j(\omega - \frac{\pi}{2T}))Q^*(j(\omega + \frac{\pi}{2T}))\right\} = 0. \tag{2.28}$$

Rewriting it in terms of the magnitude and phase of $Q(j\omega)$, we can find a constraint on the phase as

$$\cos(\theta(\omega - \frac{\pi}{2T}) + \theta(-\omega - \frac{\pi}{2T})) = 0, \quad \omega \in [-\frac{\pi}{T}, \frac{\pi}{T}], \tag{2.29}$$

or equivalently

$$\theta(\omega - \frac{\pi}{2T}) + \theta(-\omega - \frac{\pi}{2T}) = p\frac{\pi}{2}, \quad p \in \mathbb{Z} \quad \omega \in [-\frac{\pi}{T}, \frac{\pi}{T}]. \tag{2.30}$$

This implies a constraint on the phase of $q(t)$, which is easily achievable as will be explained shortly. Notice that this is exactly where the approach taken in section 2.3 failed. A comparison between Figure 2.3 and Figure 2.5 is illustrative in understanding the chain of events.

The situation with the phase requirement is depicted in Figure 2.6. Knowing

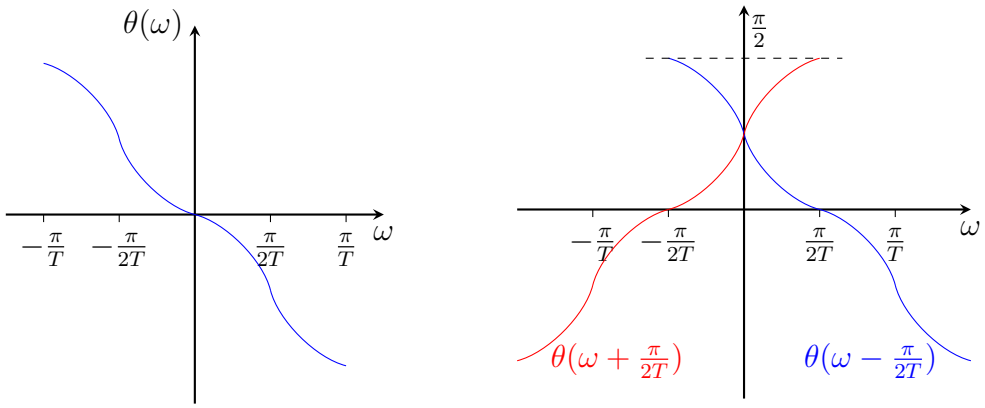

(a) (b)

Figure 2.6: An illustration of the phase constraint (2.30) imposed by the generalized Nyquist criterion. (a) A generic sketch of $\theta(\omega)$, the phase response of the basic pulse $q(t)$. (b) The terms in (2.30).

that $\theta(\omega)$ is odd, it can be seen from the figure that a phase symmetry about $\frac{\pi}{2T}$ is required. A practical consideration is to use a zero-phase or symmetric $q(t)$, where $\theta(\omega) = 0$. In this special case, the phase requirement can be met by simply adding a phase shift of $\frac{\pi}{2}$ to every other pulse. This can be readily justified by considering a multiplicative term $e^{\pm j\pi/2}$ added to either $H_n(j\omega)$ or $H_{n+1}(j\omega)$ in (2.24).

Since the developed baseband signal is real for real data symbols, hence symmetric in the frequency domain, only a single side-band is sufficient for the modulation. This way, it provides a symbol rate of $\frac{1}{T}$ for an aggregate bandwidth of about $\frac{N}{2T}$. Considering that a QAM symbol could be viewed as two real symbols, this is equal to the bandwidth efficiency of the OFDM scheme.

In order to use a single side-band, we can construct it directly without actually doing the required filtering in modulations such as VSB or SSB. This would modify the pulses to

$$h_n(t) = (q(t)e^{j\frac{\pi}{2T}t})e^{jn\frac{\pi}{T}t}, \quad n = 0, 1, \ldots, N-1. \tag{2.31}$$

The rest of the operations in such a modulator are as usual, as depicted in Figure 2.7a. The receiver, however, is slightly different. After demodulation to the baseband, the real part of the signal is obtained to form a double side-band signal. The block diagram of the receiver is depicted in Figure 2.7b.

It is now straightforward to use the CMT scheme for the QAM symbols, by splitting each into two consecutive real symbols. These real symbols are defined as

$$\begin{aligned} A'_{2k,n} &= A^R_{k,n} = \mathrm{Re}\left\{A_{k,n}\right\}, \\ A'_{2k+1,n} &= A^I_{k,n} = \mathrm{Im}\left\{A_{k,n}\right\}, \end{aligned} \tag{2.32}$$

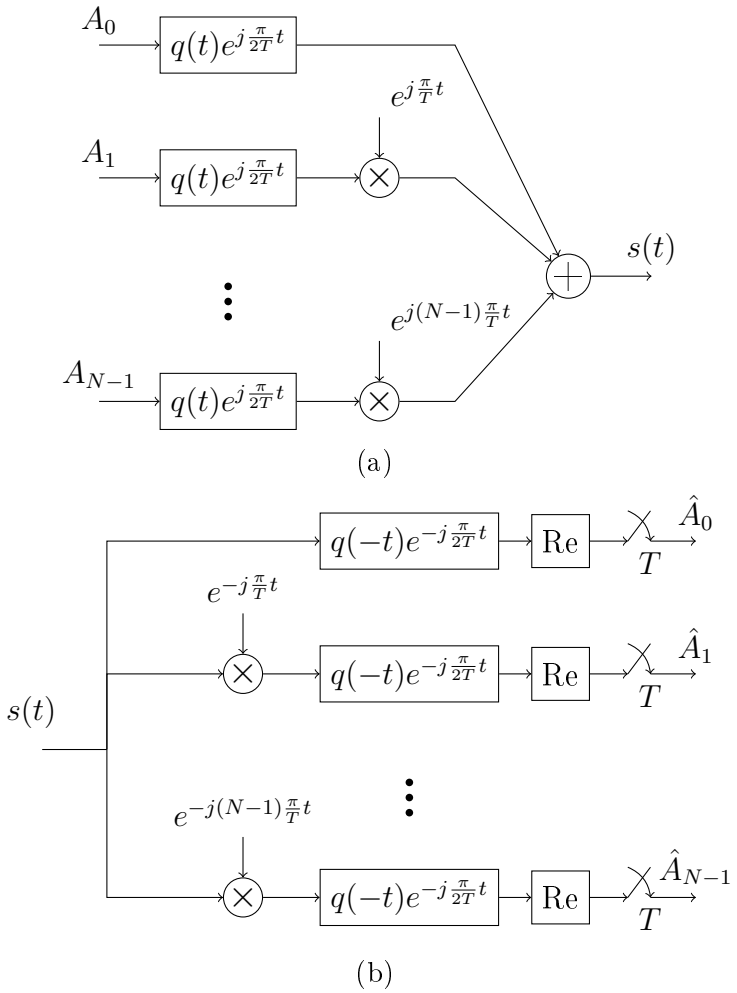

Figure 2.7: The CMT (a) modulator and (b) demodulator. Note the real operation after each filter.

where $A_{k,n}$ is the QAM symbol of time index k and subcarrier n. With the notation developed so far, such a scheme would need $2T$ for each QAM symbol. In order to adjust the parameters to the typical ones of a QAM modulation, such that the QAM symbol interval is T, consider a basic pulse $q'(t)$ which satisfies ordinary Nyquist criterion for the symbol duration of $\frac{T}{2}$. Then the minimum bandwidth of the pulse, hence the required subcarrier spacing, is $\frac{2\pi}{T}$. Therefore, we can rewrite (2.22) as

$$h'_n(t) = q'(t)\cos\left((n+\frac{1}{2})\frac{2\pi}{T}t\right), \quad n = 0, 1, \ldots, N-1, \tag{2.33}$$

or for the construction of the single side-band signal in the baseband,

$$h'_n(t) = q'(t)e^{j\frac{\pi}{T}t}e^{jn\frac{2\pi}{T}t}, \quad n = 0, 1, \ldots, N-1. \tag{2.34}$$

Figure 2.8 shows the block diagram representation of this scheme. In the diagram, a zero-phase pulse waveform is used and the generalized Nyquist criterion is satisfied

by $\frac{\pi}{2}$ phase difference between the adjacent subchannels.

2.5 Staggered Modulated Multitone (SMT)

Figure 2.9 shows an interpretation of the phase rotation $e^{j\frac{\pi}{2T}t}$ applied to the basic pulse $q(t)$ as in (2.31). It it geometrically clear that this phase rotation matches the pulse duration of T to create a phase difference of $\frac{\pi}{2}$ between the adjacent pulses. This can also be obtained mathematically by substituting (2.31) in (2.1)

$$\begin{aligned} s(t) &= \sum_{k=-\infty}^{+\infty} \sum_{n=0}^{N-1} A'_{k,n} q(t-kT) e^{j\frac{\pi}{2T}(t-kT)} e^{jn\frac{\pi}{T}(t-kT)} \\ &= e^{j\frac{\pi}{2T}t} \sum_{k=-\infty}^{+\infty} \sum_{n=0}^{N-1} A'_{k,n} q(t-kT)(-j)^k e^{jn\frac{\pi}{T}(t-kT)}. \end{aligned} \tag{2.35}$$

The term $(-j)^k$, which depends only on the time index k, implies the mentioned phase shift.

This provides an interesting insight into this development. That is, using double side-band real pulses, as the key idea behind the CMT scheme, is equivalent to applying $(-j)^k$ to the data symbols. Although it takes the values from $\{1, -j, -1, j\}$ periodically, only the $\frac{\pi}{2}$ phase difference among the adjacent subchannels is important. Therefore, a factor alternating between 1 and j is enough.

Therefore, the structure shown in Figure 2.8 can be modified to obtain the one shown in Figure 2.10. In this transformation, the derivation indicated in (2.35) is used, such that the imaginary part of the QAM symbols are now purely imaginary. In the previous structure, the effect of the phase term in the pulses were compensated by its matched filter counterpart in the receiver. In the modified scheme, the compensation is done by using the $\mathrm{Im}\{.\}$ operator instead of $\mathrm{Re}\{.\}$ for the sampling instances when a purely imaginary symbol is expected. This is equivalent to a multiplication by the suitable scalar and then using the $\mathrm{Re}\{.\}$ operator. Therefore, the working principle is unchanged.

In addition to the purely imaginary symbols, (2.35) requires multiplication of the phase term $e^{j\frac{\pi}{2T}t}$ to the time-domain baseband signal. This is equivalent to a frequency shift. However, it is immediately canceled in the receiver before the $\mathrm{Re}\{.\}$ or $\mathrm{Im}\{.\}$ operators. Therefore, they can be omitted without violating the Nyquist criteria.

The structure shown in Figure 2.10 emphasizes the idea of splitting the QAM symbols into their real and imaginary parts. That is, the input symbols of the modulator are shown at consecutive time instants. Similarly, the output symbols of the demodulator are produced based on timing of the switch. However, a more familiar appearance of this scheme, commonly known as SMT, is shown in Figure 2.11 and

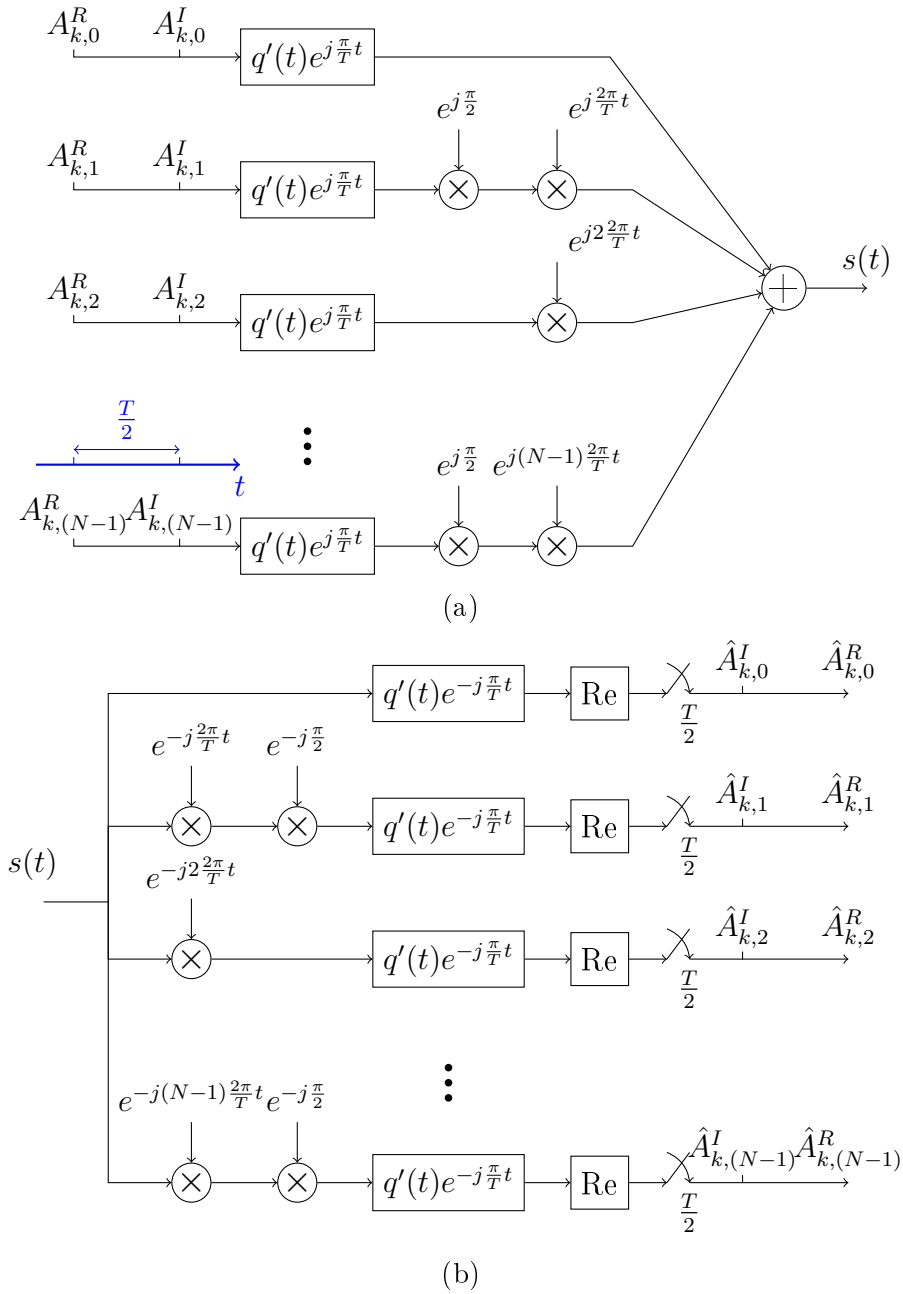

Figure 2.8: The CMT (a) modulator and (b) demodulator, for QAM data symbols and zero-phase $q'(t)$.

Figure 2.12 [9]. In this structure, the subchannel filters that process the split symbols have a time offset of $\frac{T}{2}$, implying that symbols are processed consecutively in time. The receiver filters accordingly have a time offset. Note that in the receiver, the $\mathrm{Re}\{.\}$ and $\mathrm{Im}\{.\}$ operators are commuted with the filters. This is valid as long as the filters are real, which is the case in this development.

The $e^{j\frac{\pi}{2}}$ multipliers in the SMT modulator of Figure 2.11 can be translated to a scalar j multiplied by the symbols. Thus, the QAM symbols are pre-processed before entering the modulator as shown in Figure 2.13a. It is easy to see that the

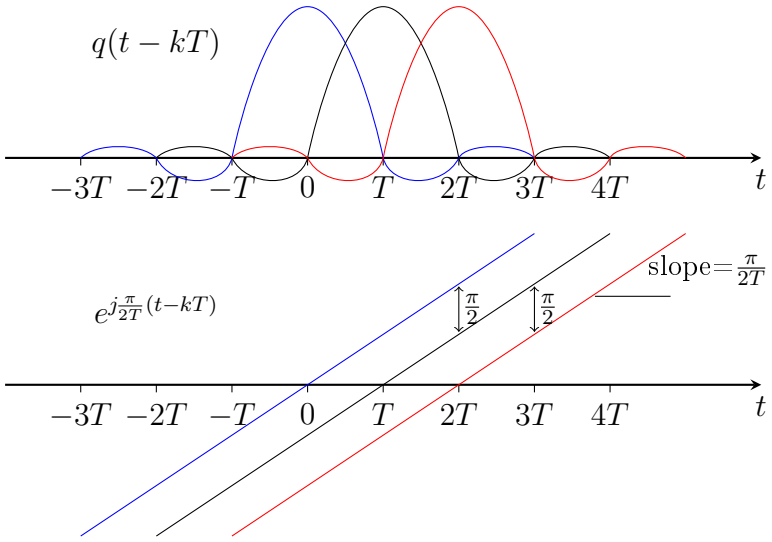

Figure 2.9: One implication of the phase rotation applied to $q(t)$ as in (2.31).

modulation works correctly if there is a phase difference of $\frac{\pi}{2}$ between the adjacent symbols on one subcarrier and between the simultaneous symbols of the adjacent subcarriers. For instance, the implementation of the PHYDYAS project [33], which is used in this work as well, is based on the phase arrangement of Figure 2.13b. In addition, the order in which the real and imaginary parts of the QAM symbols are arranged may vary. Such variations do not change the mechanism of the modulation itself, but modifies the pre- and post-processing of the QAM symbols into the so-called OQAM symbols and vice versa.

2.6 Discrete-time model, OFDM/OQAM

This chapter is concluded by introducing a practical implementation of the developed SMT scheme. The details are based on the structure used in the PHYDYAS project [33]. The SMT scheme is formalized and commonly used in the literature under the name "OFDM with offset OQAM" or OFDM/OQAM. A discrete-time version of this model is developed in [26]. It uses DFT-based modulation, as in OFDM, as well as the polyphase representation of the pulse shaping filter to achieve an efficient implementation of the OFDM/OQAM scheme.

The discrete-time model and its implementation are briefly reviewed here, mostly for the purpose of identifying how it behaves and how it must be treated in the algorithms used in the PAPR reduction methods. Therefore, the discussion here is incomplete and lacks continuity. The interested reader would find a detailed development in [26] and the required background in [32].

The discrete-time formulation of the OFDM/OQAM signal model requires causal prototype filter $h[k]$ which is the truncated and shifted version of the continuous-time

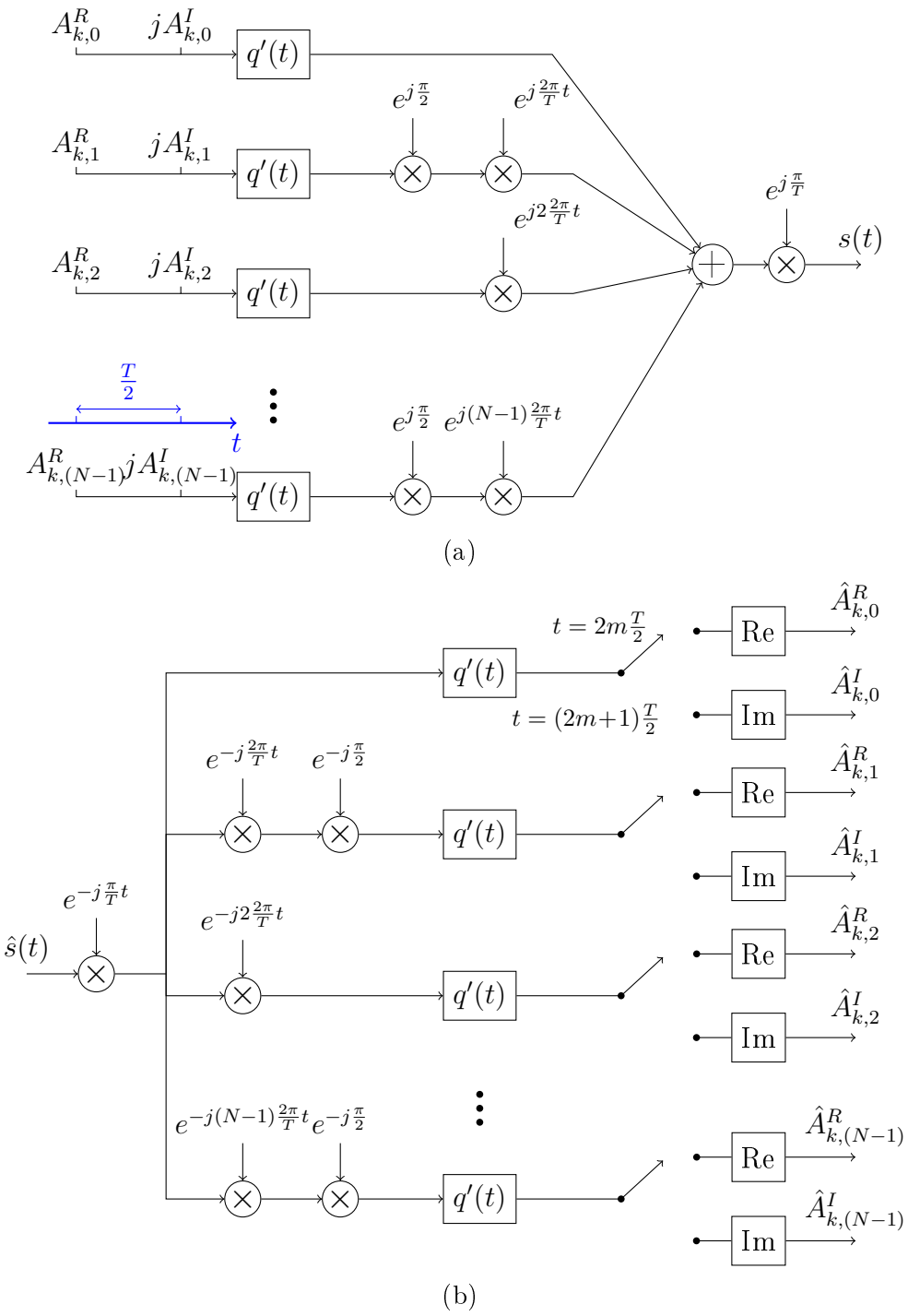

Figure 2.10: The modified CMT modulator and demodulator.

filter $h(t)$. The final discrete-time signal model is [26]

$$s[k] = \sum_{m=-\infty}^{+\infty} \sum_{n=0}^{N-1} a_{m,n} h[k - m\frac{N}{2}] e^{j\frac{2\pi}{N}n(k-D/2)} e^{j\phi_{m,n}}, \tag{2.36}$$

where the index n refers to the subcarrier number and the index m counts the

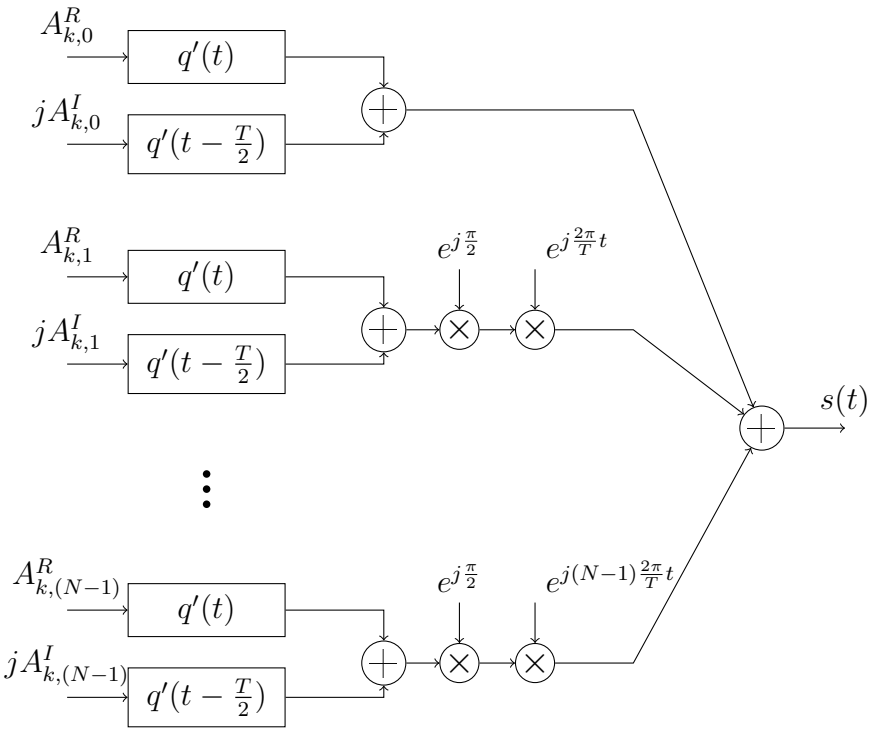

Figure 2.11: The SMT modulator.

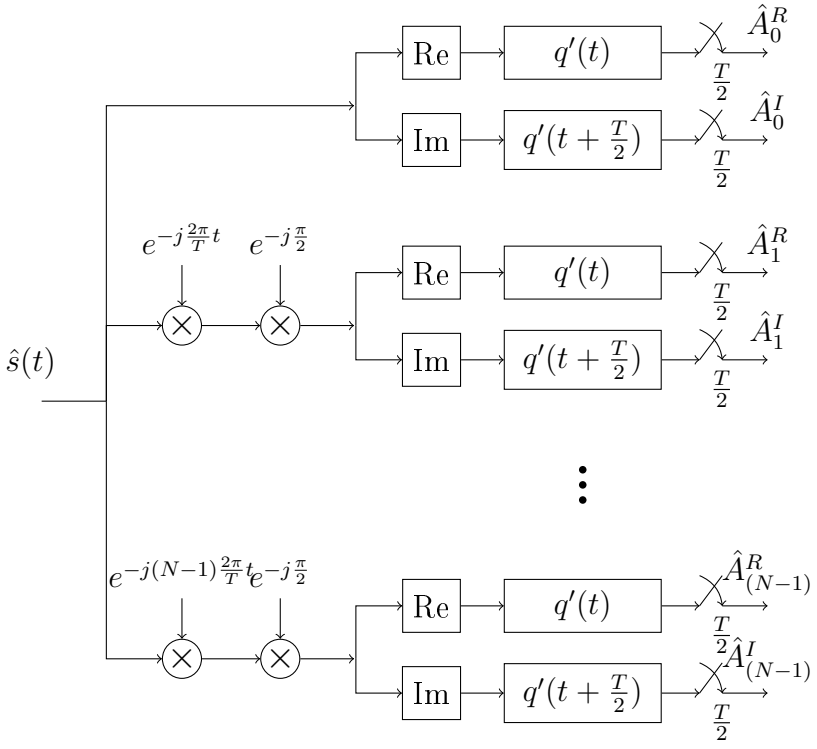

Figure 2.12: The SMT demodulator.

intervals of $\frac{N}{2}$ samples which are transmitted for each set of N OQAM symbols entering the modulator. Recall that each QAM symbol is split into two parts,

$$\begin{array}{cccc} A^R_{1,0} & jA^I_{1,0} & A^R_{2,0} & jA^I_{2,0} \\ jA^R_{1,1} & -A^I_{1,1} & jA^R_{2,1} & -A^I_{2,1} \\ A^R_{1,2} & jA^I_{1,2} & A^R_{2,2} & jA^I_{2,2} \\ jA^R_{1,3} & -A^I_{1,3} & jA^R_{2,3} & -A^I_{2,3} \end{array} \qquad \begin{array}{cccc} A^R_{1,0} & jA^I_{1,0} & -A^R_{2,0} & -jA^I_{2,0} \\ jA^R_{1,1} & -A^I_{1,1} & -jA^R_{2,1} & A^I_{2,1} \\ -A^R_{1,2} & -jA^I_{1,2} & A^R_{2,2} & jA^I_{2,2} \\ -jA^R_{1,3} & A^I_{1,3} & jA^R_{2,3} & -A^I_{2,3} \end{array}$$

(a) (b)

Figure 2.13: The preprocessing of the QAM symbols before entering the modulator, as in (a) SMT scheme, (b) implementation of the PHYDYAS project.

referred to as OQAM symbols in this text. The length of the prototype filter L_h is included in $D = L_h - 1$. The real-valued real-valued symbols $a_{m,n}$ together with the phase term $e^{j\phi_{m,n}}$ form the OQAM symbols. The conversion of the QAM symbols to the OQAM ones is illustrated in Figure 2.13. In the sequel, the efficient implementation of this model is discussed.

The modulator part, the Synthesis Filter Bank (SFB), is shown in Figure 2.14a. The inputs to the SFB are the offset QAM symbols, as shown in Figure 2.13. The IFFT block essentially performs the modulation to the subcarrier frequencies. From the hardware point of view, it performs the computations in a block processing manner. That is, a set of samples are fed into the N branches of the IFFT block at once and a set of output samples are generated. After the polyphase filters, the upsampling by a factor of $N/2$ is performed. Through the specific combination of the delays and the adders, the resulting samples from the parallel branches go through a parallel-to-serial conversion. An important point is that for a set of samples at the input of IDFT, which are one part of the two-part QAM symbols, $\frac{N}{2}$ samples are put on the final output of the SFB. Viewing from one stage before, for each set of N QAM symbols, N samples are generated at the output. However, depending on the pulse shape, each OFDM/OQAM symbol is several times longer than N samples.

The demodulator part, the Analysis Filter Bank (AFB), is shown in Figure 2.14b. The output of the parallel branches are the OQAM symbols which must go through OQAM-postprocessing which reverses the procedure shown in Figure 2.13.

One important consideration is the pulse shape, namely the prototype filter, which satisfies the orthogonality condition, i.e., the discrete-time version of the Nyquist criterion. It will be shown in section 3.3 that from the PAPR point of view, the pulse shape only needs to satisfy the orthogonality condition. Therefore, without loss of generality, the pulse shape proposed in [33] is used. Thus the impulse

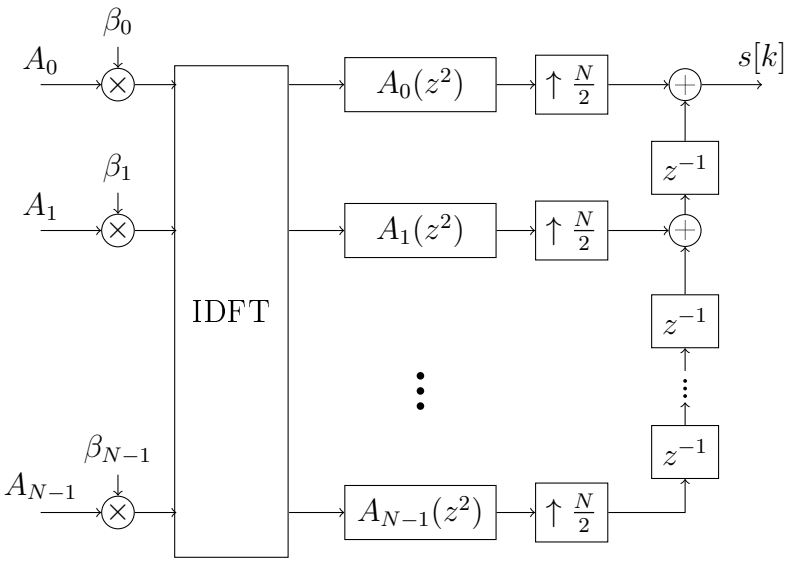

(a)

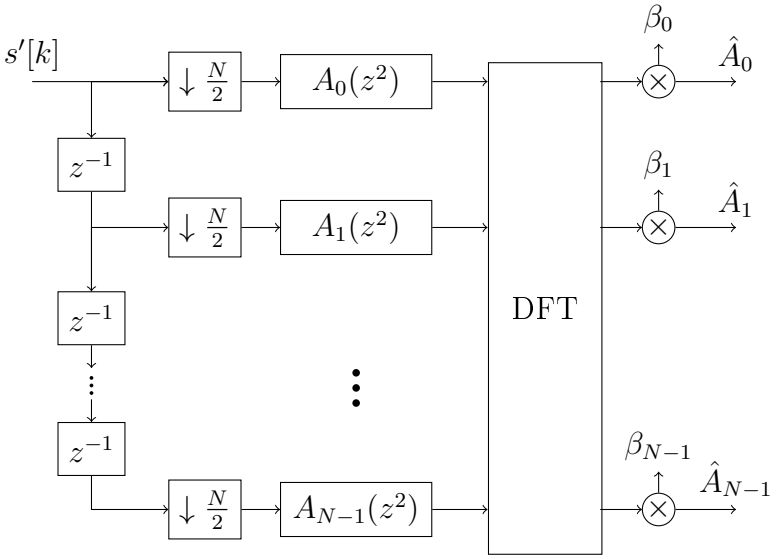

(b)

Figure 2.14: The structure of the efficient implementation of the OFDM/OQAM model. (a) The modulator or the Synthesis Filter Bank (SFB), (b) the demodulator or the Analysis Filter Bank (AFB).

response of the causal FIR prototype filter, denoted by $p[m]$, is defined as

$$p[m] = \bar{P}[0] + 2\sum_{k=1}^{K-1}(-1)^k \bar{P}[k]\cos\left(\frac{2\pi k}{KM}(m+1)\right), \quad m = 0, 1, \ldots, KM-2, \tag{2.37}$$

where M is the number of the subcarriers, $K = 4$ is the overlapping factor and the

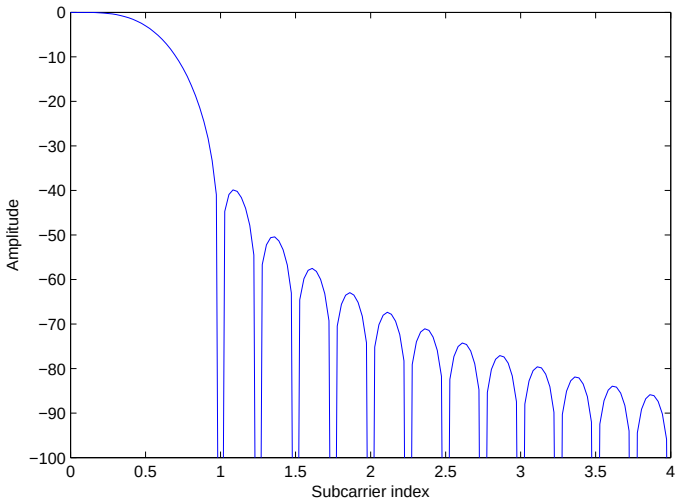

Figure 2.15: The pulse shape in the frequency domain. The frequency axis is normalized to the subcarrier spacing $\frac{2\pi}{N}$.

other constants are defined as

$$\begin{aligned}\bar{P}[0] &= 1,\\ \bar{P}[1] &= 0.97195983,\\ \bar{P}[2] &= \frac{1}{\sqrt{2}},\\ \bar{P}[3] &= \sqrt{1-\bar{P}[2]}.\end{aligned}$$

The prototype filter is designed for the fixed overlapping factor $K = 4$. This indicates that the polyphase filters and the parallel-to-serial conversion in the SFB continue processing the samples of each symbol for the following 3 symbol intervals. This time-domain overlapping will be further investigated in section 4.3. Figure 2.15 shows that the pulse shape in the frequency domain overlaps mainly over the adjacent channel, and has an attenuation of more than 60 dB afterwards.

It is evident that the discretization of the continuous-time model developed in the previous sections does not necessarily lead to perfect satisfaction of the orthogonality conditions. The described pulse shape is an example of such a design. The investigation of the details of this approximation is beyond the scope of this text. However, the mentioned literature provide an in-depth formalization of this issue and show that the interference due to the approximate orthogonality is negligible.

3. PEAK-TO-AVERAGE POWER RATIO

The waveforms of interest in modern wireless communication systems exhibit high time-domain fluctuations. When a waveform goes through nonlinear components, with some probability it exceeds the linear range. This introduces distortion to the output waveform. The nonlinearity is most troublesome with high signal levels. Therefore, power amplifier is considered to be the critical component in this discussion. The time-domain fluctuation of waveforms is typically expressed in terms of Peak-to-Average Power ratio (PAPR). This measure is then used to compare different waveforms. The methods developed to reduce the high waveform fluctuations are referred to as PAPR reduction techniques.

This chapter begins by a brief explanation of the distortion caused by the nonlinearity. Then the PAPR will be defined and investigated based on the statistical properties of the signal models. Finally, some of the important PAPR reduction techniques are reviewed.

3.1 Nonlinear distortion

The multicarrier nature of the waveforms employed in modern communication systems cause the so-called high Peak-to-Average Power ratio (PAPR). In simple words, the multicarrier waveforms have very high fluctuation in the time domain, such that the signal has large peaks and steep valleys. This ratio for the bandpass signal is about 15 dB for a typical OFDM signal, meaning that the maximum value of the instantaneous power level is about 32 times larger than its average value.

The bandpass signal must be fed into a power amplifier before being transmitted through an antenna. Power amplifiers are active nonlinear devices. In other words, they need a DC power supply and the input-output relationship is not linear over the entire possible input range. For relatively small input levels, they exhibit linear behavior, i.e., they amplify the signal by a constant gain. The input-output curve for a simplistic model of a power amplifier is shown in Figure 3.1.

As illustrated in Figure 3.1, the signal must be bounded to an interval of input power level where the device has linear behavior. Otherwise, it causes distortion. Clearly, one effect of the distortion is that the signal is changed and the underlying data symbols in the receiver cannot be detected without error. This is called the in-band distortion and leads to performance degradation. The other type of distortion

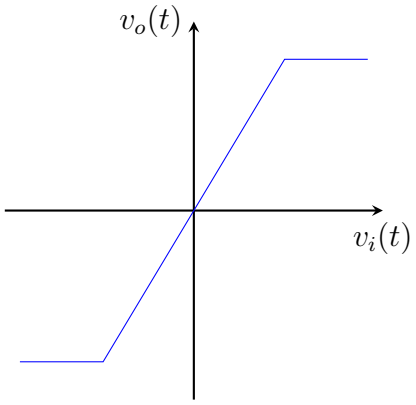

Figure 3.1: The input-output curve for a simplistic model of a power amplifier.

is due to the shape of the nonlinearity. For high signal levels, the power amplifier goes into the saturation region, where the input-output curve takes the form of a horizontal line. In other words, the signal is nearly clipped. Clipping causes sharp changes in the waveform, which in turn causes expansion in the frequency domain. In other words, the distorted signal occupies more bandwidth compared to the desired one. This is called the out-of-band distortion.

The easiest way of solving this issue is to expand the linear region of the power amplifier. This can be done either by using a power amplifier with higher power supply which has a wider linear range, or by reducing the average power of the signal, so that its peaks stay in the linear region. The latter may not be possible as it limits the transmission range. In addition, both of these methods result in poor efficiency. Apart from the energy saving aspect, it is clear that the power source is a major bottleneck in today's technology for portable devices that run on a battery. Therefore, it is necessary to reduce the PAPR of the waveforms before the power amplifier.

3.2 PAPR definition

Consider a baseband signal generated according to a modulation scheme. The signal is then up-converted and fed to power amplifier. It is most meaningful to measure the PAPR at the input of the power amplifier. However, analysis of the PAPR, either analytically or by simulations, is complicated for the RF signal. If $f_c \gg W$, where W is the bandwidth of the bandpass signal, it is a valid approximation to consider the PAPR of the baseband signal instead.

The PAPR of a continuous-time signal, denoted by γ_c, is defined over intervals of length T as

$$\gamma_c = \frac{\max\limits_{0 \le t < T} |s(t)|^2}{\mathrm{E}[|s(t)|^2]}, \tag{3.1}$$

where $|s(t)|$ is the envelope of the bandpass signal, i.e., $s(t)$ is its baseband equivalent. The numerator is the peak power of the signal and the denominator is its average power. It is clear that γ_c is a random variable. Commonly, the Complementary Cumulative Density Function (CCDF) of the random variable γ_c is used to characterize the time-domain fluctuations. The CCDF of γ_c at a specific PAPR level is the probability that γ_c exceeds that level.

However, it is important to note that the input signal of the power amplifier is the bandpass signal. The baseband signal $s(t)$ that is modulated to the carrier frequency f_c can be written in the general form of

$$\begin{aligned} s_{\mathrm{BP}}(t) &= \mathrm{Re}\{s(t)e^{j2\pi f_c t}\} \\ &= s_I(t)\cos(2\pi f_c t) - j s_Q(t)\sin(2\pi f_c t). \end{aligned} \tag{3.2}$$

The assumption of $f_c \gg W$ implies that $\max\{|s_{\mathrm{BP}}(t)|\} \simeq \max\{|s(t)|\}$ in the time intervals of interest. It can be shown that

$$\mathrm{E}\big[|s_{\mathrm{BP}}(t)|^2\big] = \frac{\mathrm{E}[|s(t)|^2]}{2}, \tag{3.3}$$

which is the denominator of the bandpass PAPR. Therefore, the PAPR for the bandpass signal is nearly twice that of the baseband signal, i.e., 3 dB higher. Since absolute values of PAPR throughout this report are not concerned, we always refer to the PAPR of the baseband signal.

The PAPR is measured over fixed intervals. In the conventional OFDM, the symbols are completely isolated in the time domain. Thus, a clear choice for the length of measurement interval is the symbol duration T. In the enhanced OFDM or OFDM/OQAM schemes, there is time domain overlapping. It is intuitively clear that by increasing the interval length for any signal, there is a higher chance of having a larger peak in each interval. As far as a measure for signal fluctuations is needed, any interval length for any signal is valid. But care must be taken to use the same interval length in comparing the time-domain characteristics of various signal models. In other words, this type of time-domain characterization concerns only the following nonlinear device, namely power amplifier. The behavior of such a component is totally independent of the underlying signal structure. Therefore, regardless of how deep the neighboring symbols overlap, this characterization is valid.

The measurement of the PAPR is required for two different purposes. It might be a part of the PAPR reduction algorithm which needs to be implemented in the hardware and has significant effect on computationally complexity of the transmitter. The second case is when PAPR is measured to determine the characteristics of the signal entering the power amplifier, or equivalently, to study performance of

the PAPR reduction method. In the former case, the measurement interval can be chosen solely based on computational convenience. However, in the latter case, it is important to do the measurement on a predetermined interval so that comparison is meaningful.

In the digital signal processing involved in the baseband part of the transmitter, PAPR measurement is done directly on the digital signal. Therefore, PAPR must be defined based on the sampled signal. A straight-forward approach is to use these samples directly to find the peak power. In the multicarrier waveforms of interest, critical sampling rate is used. Unfortunately, this rate does not capture the peaks of the signal and a minimum amount of oversampling is required. Thus, the continuous-time definition of equation (3.1) is modified as

$$\gamma_d = \frac{\max\limits_{0 \le k < LN-1} |s^{(L)}[k]|^2}{\mathrm{E}[|s^{(L)}[k]|^2]}, \tag{3.4}$$

where L is the oversampling factor. This consideration will be further studied in Chapter 5.

3.3 Statistical properties of PAPR

We are often interested in studying PAPR, as a random variable, via its CCDF. It allows us to make statements about how often or with what probability the PAPR exceeds an acceptable value. It is possible to derive approximate expressions for the CCDF of the PAPR for different waveforms. This is helpful in comparing modulation schemes in general. However, in PAPR reduction techniques, there is typically a need for measuring PAPR of a segment of the signal. By far, no analytic way of calculating PAPR has been proposed. As a matter of fact, PAPR measurement imposes a burden of computational complexity one top of the usually demanding reduction algorithms.

In this section, the CCDF of the PAPR for the waveforms of interest is investigated. The signal models developed in Chapter 2 are used here. It will be shown that the analytic expressions are not accurate as they are based on the critically-sampled signal model and, therefore, are not used very often. However, this investigation is valuable as it provides insight into the structure of the signals and to the effect of different parameters on the PAPR characteristics.

OFDM signal

The OFDM signal model in (2.13) is repeated here for convenience

$$s[k] = \frac{1}{\sqrt{N}} \sum_{n=0}^{N-1} X_n e^{j\frac{2\pi}{N}nk}, \quad k = 0, 1, \ldots, N-1. \tag{3.5}$$

It indicates that each sample $s[k]$ is obtained from summation of N scaled data symbols. In other words, each sample is the sum of a probably large number of i.i.d. complex random variables.

The instantaneous power of the critically-sampled OFDM signal is

$$\begin{aligned} |s[k]|^2 &= s[k]s^*[k] \\ &= \frac{1}{N} \sum_{n=0}^{N-1} X_n e^{j\frac{2\pi}{N}nk} \sum_{l=0}^{N-1} X_l^* e^{-j\frac{2\pi}{N}lk} \\ &= \frac{1}{N} \sum_{n=0}^{N-1} \sum_{l=0}^{N-1} X_n X_l^* e^{j\frac{2\pi}{N}(n-l)k} \\ &= \frac{1}{N} \sum_{n=0}^{N-1} |X_n|^2 + \frac{1}{N} \sum_{\substack{n=0 \\ n\neq l}}^{N-1} \sum_{l=0}^{N-1} X_n X_l^* e^{j\frac{2\pi}{N}(n-l)k} \end{aligned} \tag{3.6}$$

The mean or average power of the multicarrier waveform is proportional to the distance between the constellation points. This can be readily shown by obtaining the expected value of (3.6). It follows as

$$\mathrm{E}\big[|s[k]|^2\big] = \frac{1}{N} \sum_{n=0}^{N-1} \mathrm{E}\big[|X_n|^2\big] + \frac{1}{N} \sum_{\substack{n=0 \\ n\neq l}}^{N-1} \sum_{l=0}^{N-1} \mathrm{E}[X_n X_l^*]\, e^{j\frac{2\pi}{N}(n-l)k}. \tag{3.7}$$

A basic assumption in this context is that data symbols are identically and independently distributed. Therefore, the second term is equal to zero. Assuming that the data symbols are chosen from a constellation which is symmetric about the origin in the complex plane, thus zero-mean, $\mathrm{E}[|X_k|^2] = \sigma_X^2$ is the variance of the data symbols sequence. Therefore, the average power is

$$\mathrm{E}\big[|s[k]|^2\big] = \sigma_X^2. \tag{3.8}$$

The sum in (3.5) can be splitted into its real and imaginary parts as

$$\mathrm{Re}\,\{s[k]\} = \frac{1}{\sqrt{N}} \sum_{n=0}^{N-1} \left[\mathrm{Re}\,\{X_n\} \cos(\frac{2\pi}{N}kn) + \mathrm{Im}\,\{X_n\} \sin(\frac{2\pi}{N}kn) \right], \tag{3.9}$$

and

$$\mathrm{Im}\{s[k]\} = \frac{1}{\sqrt{N}} \sum_{n=0}^{N-1} \left[-\mathrm{Re}\{X_n\} \sin(\frac{2\pi}{N} kn) + \mathrm{Im}\{X_n\} \cos(\frac{2\pi}{N} kn) \right], \tag{3.10}$$

which are both zero mean and i.i.d. The variances $\mathrm{E}\big[\mathrm{Re}\{s[k]\}^2\big]$ and $\mathrm{E}\big[\mathrm{Im}\{s[k]\}^2\big]$ can be easily shown to be $\frac{1}{2}\sigma_X^2$.

Therefore, by the central limit theorem[1], $\mathrm{Re}\{s[k]\}$ and $\mathrm{Im}\{s[k]\}$ are both Gaussian distributed with zero mean and variance $\frac{1}{2}\sigma_X^2$. Hence, $s[k]$ is a circularly-symmetric complex Gaussian random variable[2] with variance σ_X^2. Notice that the scalar factor $\frac{1}{\sqrt{N}}$ is only necessary in the application of the central limit theorem. Otherwise, it is immaterial in most cases and also in our simulations.

We are interested in the instantaneous power of the samples of the OFDM symbols

$$|s[k]|^2 = \mathrm{Re}\{s[k]\}^2 + \mathrm{Im}\{s[k]\}^2, \tag{3.11}$$

which has the form of the Chi-square random variable with 2 degrees of freedom [21, p. 187]. Therefore, its cumulative density function is

$$\Pr\left\{|s[k]|^2 \leq \gamma\right\} = 1 - e^{-\gamma/\sigma_X^2}, \quad \gamma \geq 0. \tag{3.12}$$

In addition, it is easy to show that the samples are uncorrelated by verifying that $\mathrm{E}[s[k]s[l]^*] = \sigma_X^2 \delta_{k-l}$. Hence, the probability that the PAPR of a symbol exceeds the threshold γ_d, namely the CCDF, is obtained from the product of the related probabilities for all its samples

$$\begin{aligned} \Pr\{\gamma_d \leq \gamma\} &= 1 - \prod_{k=0}^{N-1} \Pr\left\{|s[k]|^2 \leq \gamma\right\} \\ &= 1 - (1 - e^{-\gamma/\sigma_X^2})^N, \quad \gamma \geq 0. \end{aligned} \tag{3.13}$$

It is crucial to bare in mind that all this derivation is based on the critically-sampled OFDM signal, i.e. with no oversampling. Therefore, in a sense, (3.13) is an optimistic estimate of the CCDF. The L-times oversampled OFDM signal model

[1] The central limit theorem states that: if Y is an i.i.d. scalar random sequence with mean μ and variance σ^2, then the distribution of the random sequence Z defined as $Z[n] = \frac{1}{\sqrt{n}} \sum_{k=1}^{n} (X[k] - \mu)$, will converge, as n goes to the limit, to the Gaussian distribution with a mean of zero and the same variance σ^2 [21].

[2] A scalar-valued Gaussian complex random variable $X \in \mathbb{C}$ can be considered as $\mathbf{Y} \in \mathbb{R}^2$ defined as $\mathbf{Y} = \begin{bmatrix} \mathrm{Re}\{X\} \\ \mathrm{Im}\{X\} \end{bmatrix}$, where both components are Gaussian. If the variance of $\mathbf{Y}$ can be represented as $\frac{1}{2}\begin{bmatrix} \mathrm{Re}\{Q\} & -\mathrm{Im}\{Q\} \\ \mathrm{Im}\{Q\} & \mathrm{Re}\{Q\} \end{bmatrix}$ for some non-negative $Q \in \mathbb{C}$, then X is called a circularly-symmetric complex Gaussian random variable and is specified by its mean $\mathrm{E}[X]$ and its variance Q [1].

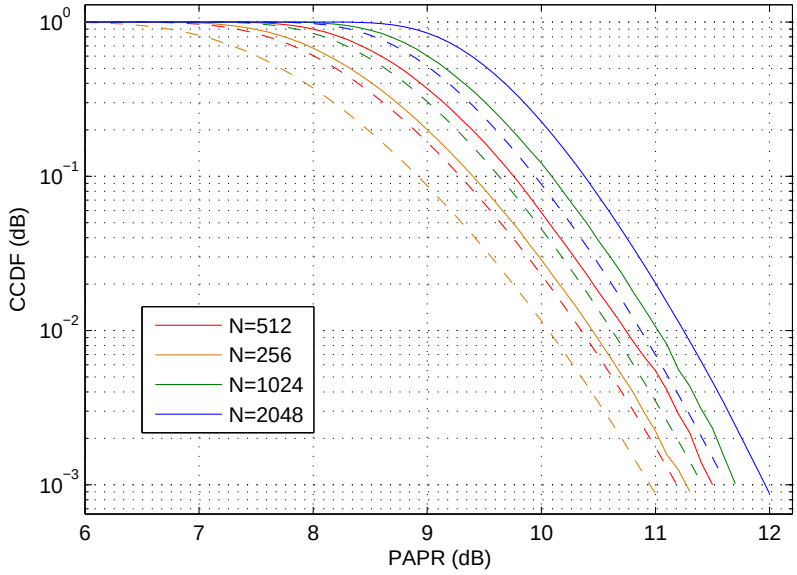

Figure 3.2: The CCDF curve for OFDM. Solid lines show simulation results for $L = 4$ and dashed lines show the analytic approximation of (3.13).

can be derived from the continuous-time model of (2.7) for $T_s = \frac{T}{LN}$ as

$$s^{(L)}[k] = \frac{1}{\sqrt{N}} \sum_{n=0}^{N-1} X_n e^{j\frac{2\pi}{LN}nk}, \quad k = 0, 1, \ldots, LN-1. \tag{3.14}$$

By investigating $\mathrm{E}\big[s^{(L)}[k]s^{(L)}[l]^*\big]$, it is evident that the oversampling causes correlation among the samples and the derivation of (3.13) is no longer valid. There has been attempts to obtain an expression for the CCDF of PAPR in oversampled OFDM signal, for instance in [16]. However, it is out of scope of this report. We always rely on simulations with sufficient oversampling.

Figure 3.2 shows the CCDF-PAPR curves for several numbers of subcarriers. The curves from the simulations and (3.13) are both included. The figure shows that the approximation of (3.13) is acceptable for a gross comparison. In addition, it shows that the PAPR characteristics get worse by increasing the number of subcarriers. However, the difference is not substantial. This indicates an important fact: even a low number of subcarriers is enough to give rise to the nonlinear distortion issue. As a rough observation, the figure suggests that by doubling the number of subcarriers, there is about 0.2 dB increase in the PAPR threshold that corresponds to the probability of 10^{-3}.

It is should be mentioned that addition of the CP has no effect on the PAPR characteristics. The CP is a copy of the ending samples of one OFDM symbol. Obviously, it cannot contain a higher peak than that of the symbol itself. Moreover, addition of the CP does not change the mean power of the symbol. Therefore, in

the subsequent discussions and in the simulations, the CP is not considered unless stated otherwise.

OFDM/OQAM signal

The analysis of the CCDF of the PAPR for the OFDM/OQAM signal is essentially similar to that of the OFDM signal. The critically-sampled discrete-time model of (2.36) is repeated here

$$s[k] = \sum_{m=-\infty}^{+\infty} \sum_{n=0}^{N-1} a_{m,n} h[k - m\frac{N}{2}] e^{j\frac{2\pi}{N}n(k-D/2)} e^{j\phi_{m,n}}. \tag{3.15}$$

In order to make the derivation easier, consider

$$s[k] = \sum_{n=0}^{N-1} s_n[k], \tag{3.16}$$

where

$$s_n[k] = \sum_{m=-\infty}^{+\infty} a_{m,n} h[k - m\frac{N}{2}] e^{j\frac{2\pi}{N}n(k-D/2)} e^{j\phi_{m,n}}, \tag{3.17}$$

which is the signal on the n^{th} subcarrier. Notice that $a_{m,n}$'s are, possibly permuted, real or imaginary components of the i.i.d. QAM symbols. Thus they are uncorrelated and have a variance of $\sigma_a^2 = \frac{1}{2}\sigma_X^2$.

It is easy to show that $s_n[k]$'s are uncorrelated, $\mathrm{E}[s_n[k]] = 0$ and finally

$$\sigma_s^2 = \mathrm{E}[s_n[k] s_n^*[k]] = \sigma_a^2 \sum_{m=-\infty}^{+\infty} h[k - m\frac{N}{2}]. \tag{3.18}$$

This makes it possible to employ the central limit theorem, as in the analysis of the OFDM signal, to conclude that $\mathrm{Re}\{s[k]\}$ and $\mathrm{Im}\{s[k]\}$ are of Gaussian distribution with zero mean and identical variance of $N\frac{\sigma_s^2}{2}$. Thus $s[k]$ is a circularly-symmetric complex Gaussian random variable with a variance of $N\sigma_s^2$. Notice that by the central limit theorem, the variance of $\frac{1}{\sqrt{N}}s[k]$ is σ_s^2. Thus the variance of $s[k]$ is N times larger.

Similar to the case of the OFDM signal, using the Chi-square distribution with 2 degrees of freedom, it can be shown that [29]

$$\Pr\left\{\frac{|s[k]|^2}{\mathrm{E}[|s[k]|^2]} \leq \gamma\right\} = 1 - e^{-\alpha_k \gamma}, \tag{3.19}$$

where

$$\alpha_k = \frac{2}{N \sum_{m\in\mathbb{Z}} h[k - m\frac{N}{2}]^2}. \tag{3.20}$$

Therefore, the CCDF of the PAPR for the critically-sampled OFDM/OQAM signal is

$$\Pr\{\gamma_d \geq \gamma\} = 1 - \prod_{k=0}^{M-1} (1 - e^{-\alpha_k \gamma}), \tag{3.21}$$

which generally depends on the sample number k in each block of M samples. Specifically, the set of parameters $\{\alpha_0, \alpha_1, \ldots, \alpha_{M-1}\}$ depend on the pulse shape $h[k]$.

In addition, it is proved in [29] that in the interesting range of PAPR thresholds, the CCDF is minimized if the orthogonality condition of the prototype filter is satisfied. Finally, this optimality results in a CCDF which is identical to that of the OFDM. Since the practical prototype filters are orthogonal to a good extent, it is assumed in this text that the PAPR is minimized from the this aspect. It can be easily verified by simulations that the PAPR characteristics of the OFDM and OFDM/OQAM waveforms are similar.

3.4 PAPR reduction techniques

In this section, some of the mainstream techniques that have been proposed in the past three decades with the objective of reducing the PAPR of the OFDM symbols are briefly introduced. They mostly fall into two categories of distortion-based techniques and multiple signal representation techniques [11]. Most of these methods are not directly applicable to the OFDM/OQAM signal model. More thorough study and comparison of the PAPR reduction techniques can be found in the literature, in particular [11].

In the distortion-based techniques, the general idea is to allow a certain level of distortion in a controlled manner, so that the performance of the system is maintained. On the other hand, the idea behind the multiple signal representation is to manipulate the data symbols such that the PAPR of the resulting OFDM symbol is reduced. The modifications to the data symbols are then reversed in the receiver. The techniques in the latter category generally have higher computational complexity due to their algorithmic and iterative nature, as will be explained in more details shortly.

In the distortion-based techniques, the term "reduction" might be somewhat misleading as the PAPR of the OFDM symbols is not really reduced. In fact, instead of letting the signal get distorted by the nonlinear amplifier, a controlled and deliberate distortion is introduced to the signal.

Clipping and Filtering

The possibly earliest method proposed to avoid the nonlinear distortion of the power amplifier is based on deliberate clipping of the signal beforehand [19]. This simple idea, supported by some enhancements after the clipping, can provide acceptable performance. There has been many modifications and improvements to the method, both in the transmitter and the receiver side, for instance in [6; 12; 25]. However, only the main ideas in the transmitter side are briefly reviewed here.

In principle, the signal which enters the power amplifier must be limited to a maximum PAPR to avoid the distortion. Therefore, the deliberate clipping could be considered on the continuous-time signal after the up-conversion or after the D/A. In practice, however, the baseband discrete-time signal is clipped. Although there could be various clipping methods [10], a typically mentioned one is the soft envelope limiter and is defined as

$$\tilde{s}[n] = \begin{cases} s[n] & \rho_n \leq A \\ Ae^{j\phi_n} & \rho_n > A, \end{cases} \tag{3.22}$$

where $s[n] = \rho_n e^{j\phi_n}$ is a sample of the baseband signal and A is the clipping level. Clearly, the performance degradation, namely the detection error rate, is directly affected by the clipping level. A trade-off is finally required between the reduction in the PAPR and the tolerable detection error rate.

Consider the clipping of the continuous-time signal, of which $s[k]$ is a sampled version. The clipping causes sharp behavior in the waveform, which is equivalent to a spread-out frequency content. Therefore, a higher sampling rate might be required. In other words, if the clipping is perform on the critically-sampled multicarrier signal, considerable aliasing would happen because the out-of-band radiation that folds back on the signal is of relatively high energy. This causes a limiting in-band distortion. In addition, the lowpass filtering of the D/A conversion causes considerable peak-regrowth [17]. As a conclusion, clipping is normally performed on the oversampled signal.

If the clipping is performed on a signal with high enough oversampling, the out-of-band radiation that falls back on the main signal band is tolerable. However, the signal must be filtered to remove the out-of-band content. This filtering can be done in the frequency domain by a pair of DFT-IDFT blocks. That is, the frequency bins that fall out of the signal band are forced to zero. This ideal lowpass filtering causes peak-regrowth, which is, however, much smaller than in the case of critically-sampled signal.

Selected Mapping (SLM)

The OFDM symbol can be viewed as the sum of a relatively large number of complex exponentials with random amplitude and phases. At different time instants, the complex exponentials, which can be considered as vectors, may add constructively or destructively. This is the reason behind the high time-domain fluctuations of the OFDM signal. It is intuitively convincing that changing the phase of the underlying data symbols changes the PAPR of the symbol to a possibly lower level.

The Selected Mapping (SLM) technique [3] is based on this idea. The data symbols are multiplied in a symbol-wise manner by several predefined sets of phase rotation terms. These complex scalars are of the form $e^{j\phi}$. Then each mapping is converted to the OFDM symbol through an IFFT block. Finally the mapping with the minimum PAPR is selected and transmitted. The phase rotations are canceled in the receiver before the detection.

Generating each mapping in the SLM technique needs one IFFT block. If the number of branches required to gain the desired PAPR reduction is high, the computational complexity of the method becomes impractical. This method, clearly, causes no distortion to the signal. The average power is also left unaltered as the phase terms are of unit amplitude. This method will be further investigated in Chapter 4.

Partial Transmit Sequences (PTS)

The Partial Transmit Sequences (PTS) technique [15] is the computationally efficient successor of the SLM technique. The idea is to perform the phase rotation on groups of subcarrier symbols instead of every one of them. That is, in order to generate a mapping, the data symbols are partitioned into several groups and each one of them undergoes a single phase rotation.

The DFT is a linear operation. Therefore, multiplication of all the time domain samples after the IDFT by a phase term translates directly to the underlying data symbols. In addition, setting the rest of the symbols to zero, each group of subcarriers can be transformed by one IFFT block separately and finally summed up to obtain the final OFDM symbol.

Therefore, each group of subcarriers is first transformed to a so-called Partial Transmit Sequence (PTS). Then the phase rotations are performed in different orders on these PTS's. The point is that the IFFT blocks are used only once. In comparison to the SLM technique, it can be shown by simulations that this method gives a similar PAPR reduction by a much lower computational complexity. This technique will be further investigated in Chapter 4.

Tone Reservation (TR)

In the Tone Reservation (TR) technique [30], as the name suggests, a number of subcarriers are reserved for the purpose of PAPR reduction. These subcarriers are modulated by a chosen set of values such that the PAPR is reduced, possibly to an optimum or sub-optimum level. Some aspects of this method are: how to choose the non-data-bearing subcarriers, what the set of possible values for these subcarriers is and finally how to find the best set of values for a specific OFDM symbol. The procedure must be repeated for each OFDM symbol and the computational complexity could be impractical for a high level of PAPR reduction.

Clearly, the TR technique provides the PAPR reduction in expense of a loss in the throughput or the spectral efficiency. In the communication systems where the channel state is known or can be estimated and fed back to the transmitter, the subcarriers used for this technique can be located where the channel has a severe attenuation. This way there will be no loss in the spectral efficiency. One advantage of this technique is that the only required information in the receiver is the location of the reserved subcarriers, which is either pre-fixed or is acquired from an otherwise beneficial exchange of information between the transmitter and the receiver.

Tone Injection (TI)

In the Tone Injection (TI) technique [30], the idea is to change the amplitude and phase of the data symbols on all the subcarriers such that the PAPR is reduced. This is done by considering an expanded constellation. Each point in the original constellation can be mapped to a set of points in the expanded one. These sets are disjoint, thus the detection in the receiver is possible. The computational complexity of the method depends on the number of points in the expanded constellation and the algorithm chosen to find the optimum or sub-optimum mappings. Similar to other iterative algorithms, the complexity could become quickly impractical for the desired levels of PAPR reduction.

The TI technique is advantageous in the sense that no loss in the spectral efficiency is imposed and no side-information is necessary in the receiver. However, as the number of points in the constellation is increased, the average signal power could be considerably higher than the original one. In other words, the PAPR reduction is gained in expense of an increase in the transmission power.

4. SLM-LIKE TECHNIQUES

The Selected Mapping (SLM) and, its successor, the Partial Transmit Sequences (PTS) techniques are the main representatives of a class of PAPR reduction techniques which are based on phase rotations on the underlying data symbols. This report mainly aims at investigating these approaches.

In this chapter, the SLM and PTS techniques are studied in details. They are firstly described in the context of the OFDM signal model, for which they were originally proposed. Applicability of these ideas to the OFDM/OQAM signal model will be then considered.

4.1 Selected Mappings (SLM)

For an OFDM symbol, as studied in section 3.3, the CCDF of the PAPR is

$$\Pr\{\gamma_d > \gamma\} = 1 - (1 - e^{-\gamma})^N, \tag{4.1}$$

which is based on the fact that each sample of an OFDM symbol is the sum of N statistically independent random variables and, by central limit theorem, has a Gaussian distribution. This assumption is a valid one as the number of subcarriers typically considered is quite high. However, time-domain samples of OFDM symbol generated at Nyquist rate do not capture the peaks accurately. It is well-known that oversampling is required, which causes statistical dependence between neighboring samples and hence (4.1) no more holds. However, it gives an optimistic CCDF, which could be insightful.

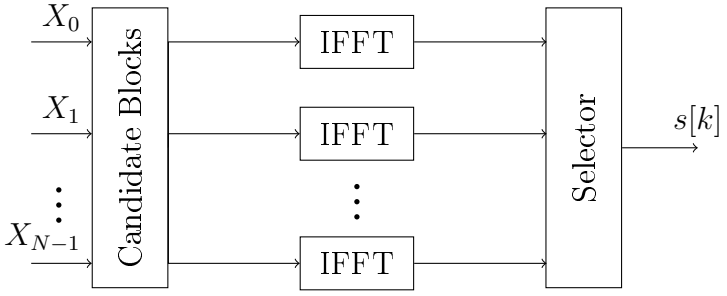

Figure 4.1: The structure of the SLM technique.

The SLM technique is based on choosing the sequence with minimum PAPR from

M candidate sequences, all of which representing the same block of N data symbols [3]. Assuming that M statistically independent OFDM symbols are generated based on the same data symbols, it is easy to see that

$$\Pr\{\gamma_d > \gamma\} = \left(1 - (1 - e^{-\gamma})^N\right)^M . \tag{4.2}$$

This gives almost an upper bound on the capability of the schemes based on the SLM idea. The challenge is then to come up with a method to generate the candidate sequences, which requires reasonable computational resources and results in as "independent" as possible sequences.

The method suggested by [3] is to multiply the block of data symbols X_k for $k = 0, \ldots, N-1$, in a point-wise manner, by M different sequences

$$P_m = [e^{j\phi_1^m}, \ldots, e^{j\phi_N^m}] \qquad m = 1, 2, \ldots, M \tag{4.3}$$

where the phases ϕ_i^m are randomly chosen from $[0, 2\pi)$. The corresponding OFDM symbols must be then generated by M separate IFFT blocks. This readily reveals the high computational complexity of this method. The structure of this technique is depicted in Figure 4.1. The oversampling is done by using a larger FFT block and inserting zeros to the data sequences. A more complete discussion of the oversampling and the alternative ways is provided in Chapter 5.

In the receiver, the phase rotations must be reversed. Thus the used phase values must be available in the receiver. Therefore, using a fixed set of phase sequences makes more sense in terms of the amount of side-information, or equivalently the loss in the throughput. Otherwise, an option is to randomly generate M sets of phase sequences for each OFDM symbol.

Obtaining the phase sequences that result in the best PAPR reduction, or in other words, finding the optimality condition of the phase sequences has attracted considerable attention in research community. For instance, this problem is addressed in [18] and [35], among many other research papers. However, from the practical point of view, the PAPR reduction capability of the technique can be estimated by a number of simulations. In addition, a SLM technique without side-information is proposed in [4].

For various values of M, complex phase terms of the sequences are generated: 1. from a uniform distribution in the interval $[0, 2\pi)$, 2. uniformly from the set $\{1, j, -1, -j\}$ and 3. uniformly from the set $\{1, -1\}$. The latter two cases have the interesting feature of avoiding complex multiplications. In all the simulations, the phases are generated once and used in the algorithm for all the OFDM symbols. In addition, one of the M candidate sequences of the SLM technique is always taken as the original sequence.

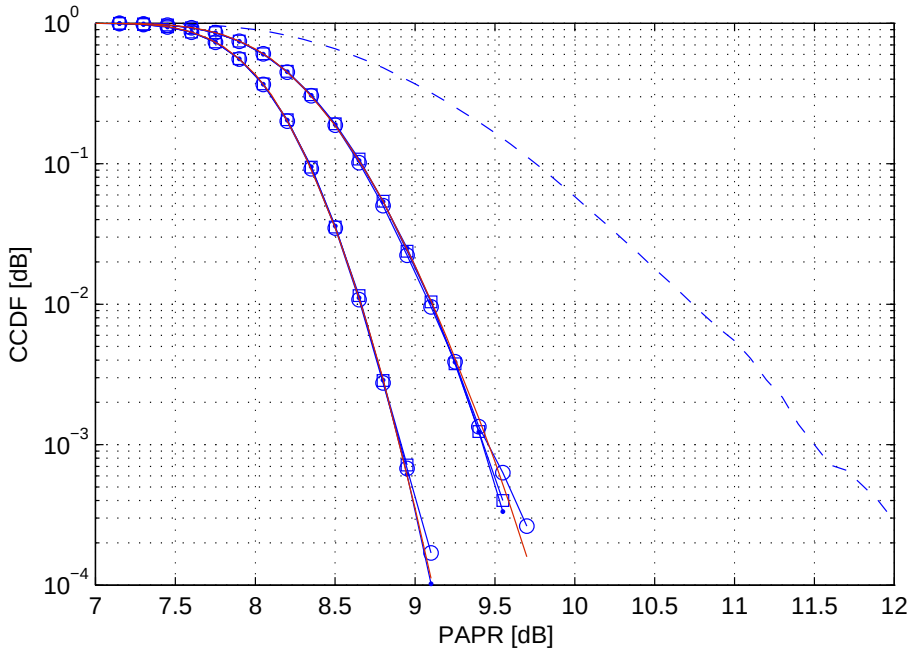

Figure 4.2: The PAPR reduction capability of the SLM technique against the theoretical upper bounds, the red curves, for $M = 4$ and 8 branches.

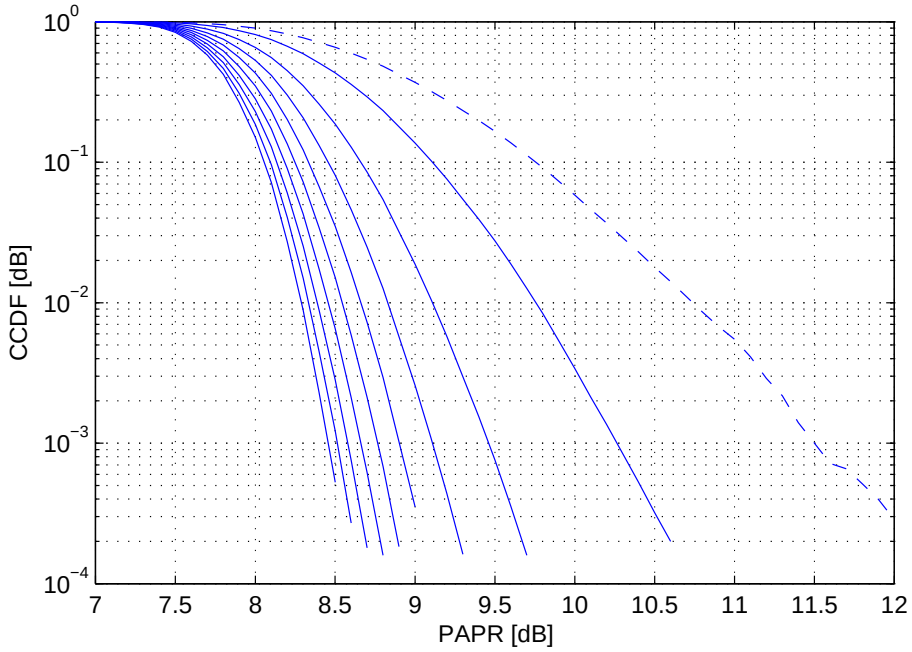

Figure 4.3: The theoretical upper bound on performance of the SLM technique, the solid curves, obtained in a similar manner to that of Figure 4.2. From right to left: $M = 2, 4, 6, \ldots, 16$

The simulation results for $N = 512$ are shown in Figure 4.2, where the PAPR reduction for $M = 4$ and 8 branches by the SLM technique is considered. The red

curves indicate the theoretical upper bounds. Here, inspired by the analytic result of (4.3), the CCDF curves of the original OFDM signals obtained from simulations are raised to the power of M. The aforementioned choices of the phase sequences, the solid blue lines, are distinguished by different markers. However, as shown in the figure, they all closely match. More insight on the effect of the phase sequences on the PAPR reduction will be revealed by studying the PTS method in the next section. Sufficing to the argument given on recognizing the red curves in Figure 4.2 as the theoretical upper bounds on the performance of the SLM technique, they are depicted for a wider range of the values of M in Figure 4.3.

4.2 Partial Transmit Sequences (PTS)

The SLM technique becomes computationally very demanding because it needs several IFFT blocks to give good PAPR reduction. In the SLM technique, the phase sequences are first multiplied by the data symbols and then the candidate OFDM symbols are generated. In the PTS technique [15], the idea is to apply the phase rotations on the time-domain signal after a small set of IFFT blocks. This indeed limits the resolution of this process, but it will be shown that it gives interesting performance.

In the PTS technique, the data symbols are partitioned into several groups, called subblocks. Considering the location of the data symbols in the frequency domain, these subblocks could be disjoint or interleaved. In addition, the partitioning could be done randomly for each OFDM symbol. However, for practical purposes, as well as simplicity of the notation, only the case of disjoint and fixed subblocks is studied. The more general setting leads to better PAPR reduction, but is not interesting in practice, as it would require a high amount of side-information and processing.

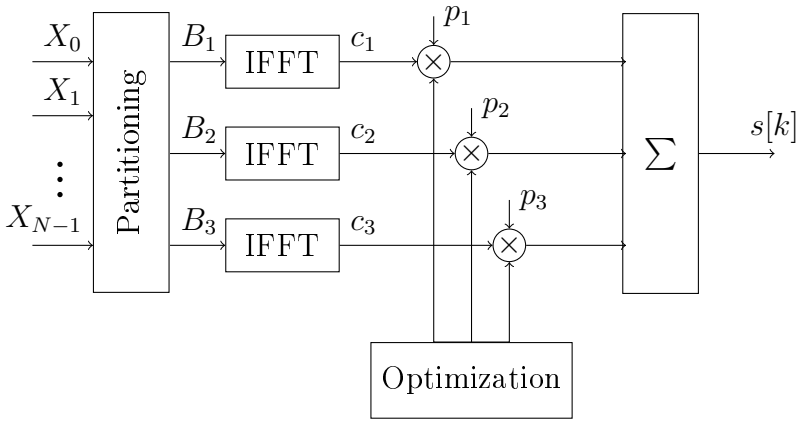

Figure 4.4: The structure of the PTS technique.

The technique will be described through an example of $M = 3$ subblocks to make the explanations simpler. Consider that the data symbols $[X_0, X_1, \ldots, X_{N-1}]$ are

partitioned into three subblocks as

$$[X_0, X_1, \ldots, X_{N_1-1}], [X_{N_1}, \ldots, X_{N_1+N_2-1}], [X_{N_1+N_2}, \ldots, X_{N_1+N_2+N_3-1}] \tag{4.4}$$

where $N = N_1 + N_2 + N_3$. The missing data symbols are replaced by zeros to form

$$\begin{aligned} B_1 &= [X_0 \ldots, X_{N_1-1}, \underbrace{0, 0, \ldots, 0}_{N_2}, \underbrace{0, 0, \ldots, 0}_{N_3}] \\ B_2 &= [\underbrace{0, 0, \ldots, 0}_{N_1}, X_{N_1+1} \ldots, X_{N_1+N_2+1}, \underbrace{0, 0, \ldots, 0}_{N_3}] \\ B_3 &= [\underbrace{0, 0, \ldots, 0}_{N_1}, \underbrace{0, 0, \ldots, 0}_{N_2}, X_{N_1+N_2} \ldots, X_{N-1}]. \end{aligned} \tag{4.5}$$

These sequences are then fed into $M = 3$ IFFT blocks to obtain the so-called partial transmit sequences c_i for $i = 1, \ldots, M$. Multiplication of c_i by a complex phase term is equivalent to phase rotation of the underlying data symbols in c_i by the same amount. For instance, for c_2, we have

$$c_2[k] = e^{j\phi} \sum_{n=0}^{N-1} B_{2,n} e^{j2\pi kn/N} \tag{4.6}$$

$$= e^{j\phi} \sum_{n=N_1+1}^{N_1+N_2-1} X_n e^{j2\pi kn/N} \tag{4.7}$$

$$= \sum_{n=N_1+1}^{N_1+N_2-1} (X_n e^{j\phi}) e^{j2\pi kn/N}. \tag{4.8}$$

Moreover, due to the linearity of the IDFT, it is possible to sum c_i's to obtain the whole OFDM symbol at the end.

Therefore, it's possible to do the phase rotations on groups of data symbols directly in the time domain. In other words, several sets of M phase rotations could be applied to the M subblocks without performing the IFFTs again. The structure of the PTS technique is depicted in Figure 4.4. As in the case of the SLM technique, the oversampling consideration are taken into account by a larger IFFT size and will be elaborated in Chapter 5.

The phase rotations could be performed with considerable algorithmic flexibility. Consider the set of W possible phase terms

$$\Phi = \{e^{j\phi_1}, e^{j\phi_2}, \ldots, e^{j\phi_W}\}. \tag{4.9}$$

The simplest way of apply the rotations is to exhaustively try all the possible phase combinations. The first phase term can be fixed to unity with no loss in perfor-

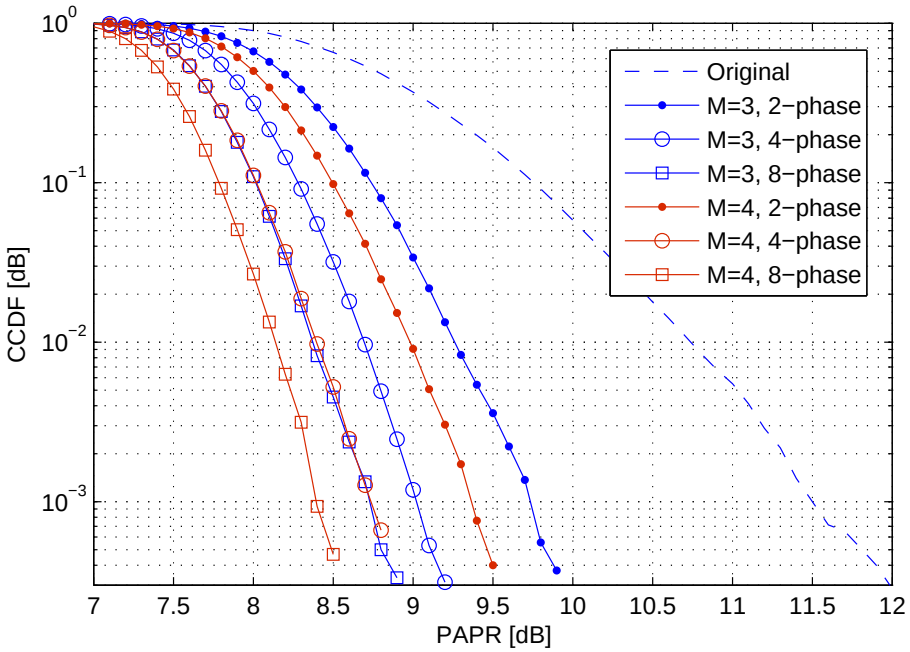

Figure 4.5: Performance of the PTS technique for fully-loaded OFDM with $N = 512$. 2-, 4- and 8-phase refer to $\{1, -1\}$, $\{1, j, -1, -j\}$ and $\{1, e^{j\frac{\pi}{4}}, \ldots, e^{j7\frac{\pi}{4}}\}$, respectively.

mance. Therefore, there are W^{M-1} possible combinations. There are various other optimization methods suggested in the literature, for instance the iterative flipping algorithm [7]. In this report, the exhaustive search is used, as for the considered values of M and the practical phase set $\Phi = \{1, j, -1, -j\}$, the complexity remains acceptable.

The number of candidate sequences increases for higher M and W. Thus it is intuitively sensible that a higher PAPR reduction is expected. Comparing the performance of the PTS and SLM techniques is insightful about the main idea of generating statistically different candidate sequences. A number of simulations are carried out for fully-loaded OFDM signal with $N = 512$ subcarriers, the result of which is depicted in Figure 4.5.

For instance, the PTS technique for $M = 3$ and $\Phi = \{1, j, -1, -j\}$, which generates 16 candidate sequences, gives a PAPR reduction of about 2.5 dB. The same gain by the SLM technique is achieved by using $M = 8$ branches. Considering that this choice of the phase terms prevents from complex multiplications, the computational complexity of using the SLM technique is drastically higher. Another observation is that for 16 candidate sequences, the SLM technique would yield a reduction of about 3 dB, which in comparison to the 2.5 dB reduction of the equivalent PTS technique is not high enough to compensate for the humongous computational complexity. In addition, the diversity of the phase sequences in this setting of the PTS technique is far lower. In the sequel, the case of $M = 3$ subblocks and $\Phi = \{1, j, -1, -j\}$ will

be the frequently used.

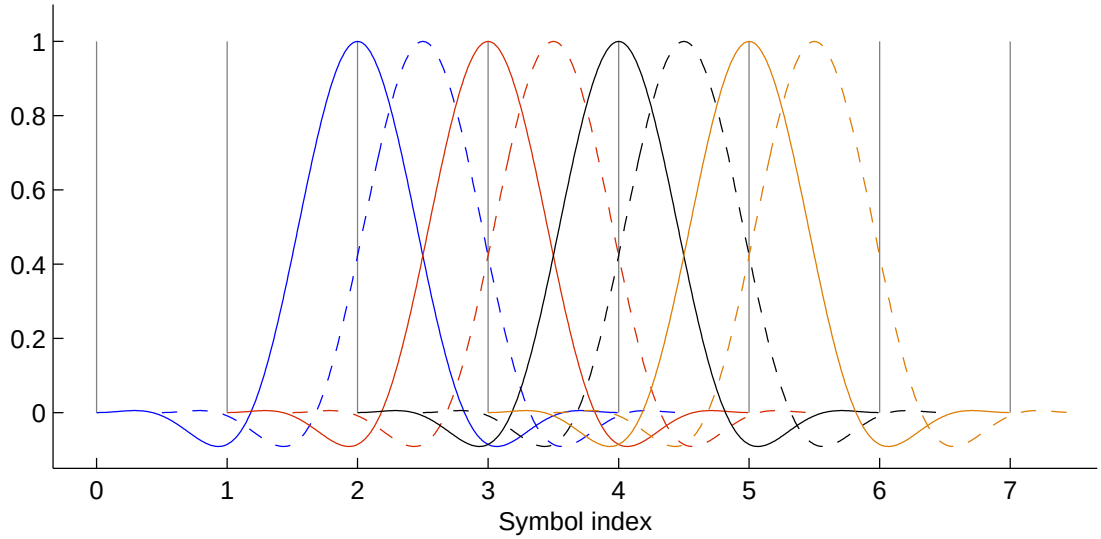

Figure 4.6: Illustration of how the pulses overlap for 4 consecutive OFDM/OQAM symbols.

4.3 Application to the OFDM/OQAM

A fundamental difference between the OFDM and the OFDM/OQAM signal models, as elaborated in Chapter 2, is that there is no overlapping in the time domain among the symbols of the former, while those of the latter could overlap over several symbols. The PAPR reduction methods proposed in the literature have been originally developed for the OFDM signal model. In other words, the processing required for PAPR minimization of each symbol is done independently. This makes the algorithms considerably simpler and less complex. Adapting these techniques to the new modulation schemes is not straight-forward.

The OFDM/OQAM discrete-time model of (2.36) is repeated here for convenience:

$$s[k] = \sum_{m=-\infty}^{+\infty} \sum_{n=0}^{N-1} a_{m,n} h[k - m\frac{N}{2}] e^{j\frac{2\pi}{N}n(k-D/2)} e^{j\phi_{m,n}}, \tag{4.10}$$

Each OFDM/OQAM symbol, generated based on N QAM symbols, consists of two subsymbols that are processed $\frac{N}{2}$ samples apart. As described in Chapter 2, a set of N QAM symbols are converted into two sets of N OQAM symbols, denoted by the combination of the variables $a_{m,n}$ and the phase terms $e^{j\phi_{m,n}}$. In this discussion, K is the overlapping factor.

Figure 4.6 shows how the pulses overlap for 4 consecutive OFDM/OQAM symbols, that is 8 modulated pulses. In this figure, the pulse shapes are only illustrating

the beginning and ending of the N-sample intervals. As shown, the first pulse, the solid blue curve, spreads out to $4N$ samples. The next pulse shown by the dashed blue curve, which belongs to the same OFDM/OQAM symbol, starts $\frac{N}{2}$ samples later and reaches $(4+\frac{1}{2})N$.

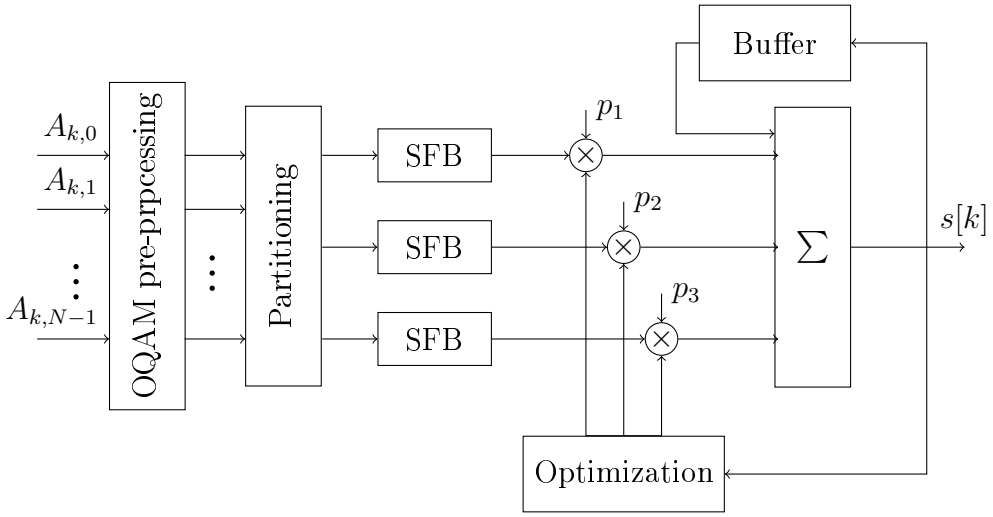

Figure 4.7: Structure of the PTS technique with 3 subblocks, modified for the OFDM/OQAM signal.

To illustrate the challenge, a naive adaptation of the PTS technique to the OFDM/OQAM signal model is presented. Reminding the structure of Figure 4.4, the phase rotations are performed directly on the time-domain partial transmit sequences. To follow the idea, time-domain multiplication can only be done on isolated pulses. In other words, 1) transferring the phase rotations to the underlying data symbols needs the whole OFDM/OQAM symbol. 2) since in the time domain, the samples are a combination of present and past symbols, phase rotation is not directly possible and violates the orthogonality of the modulation scheme.

Since the modulation is actually done on the OQAM data symbols, the presented PTS technique performs the process for each set of OQAM symbols, i.e., every $\frac{N}{2}$ sample. To make the described idea work, it is necessary to modify the Synthesis Filter Bank (SFB) discussed in Section 2.6, such that after one normal operation, the parallel polyphase filters, the upsamplers, etc. are fed by zeros for long enough such that the whole KN samples are produced in the output. After the optimization process for this isolated symbol, the buffered $KN - \frac{N}{2}$ past samples must be added to the beginning of the symbol. The first $\frac{N}{2}$ samples of the result is ready for transmission and the remaining $KN - \frac{N}{2}$ is buffered.

The structure of the described PTS scheme is depicted in Figure 4.7. Concerning the optimization process, the addition of the buffered samples must be performed before the PAPR measurement. For the sake of efficiency, and considering the relatively weak tails of the usual pulse shapes, the PAPR measurement in a part of the

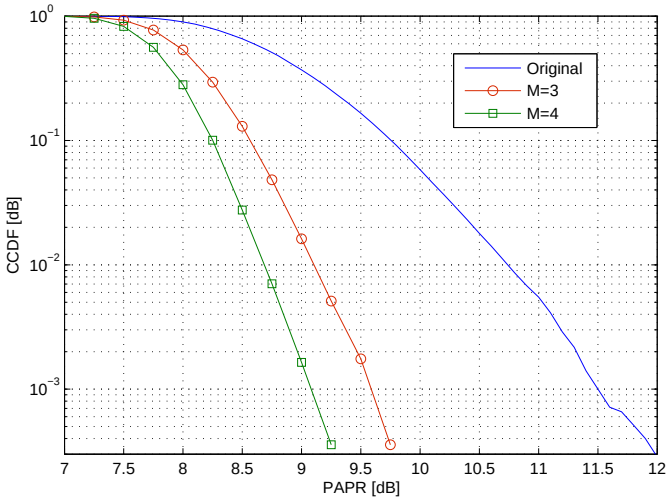

Figure 4.8: The CCDF curved obtained from the PTS technique modified for the OFDM/OQAM signal; simulated for $N = 512$, $M = 3$ and 4 disjoint subblocks of equal size and the phase set $\{1, -1\}$.

available KN samples could lead to the same performance. One important consideration is that the phase of the OQAM symbols is specifically chosen and cannot be changed without violation of the orthogonality of the modulation. Therefore, the phase terms are limited to $\{-1, 1\}$. Considering the motivation behind the phase arrangements, as elaborated in section 2.5, and the typical assumption of 100% roll-off in the pulse design, it must be sufficient to leave one subcarrier empty between the PTS subblocks to make arbitrary phase rotations feasible. However, this would require a modification to the normal OQAM post-processing block.

The PAPR reduction gained by this scheme is shown by the CCDF curves in Figure 4.8. The performance is very close to that of the PTS technique for the OFDM signal. However, the added complexity due to the multiple SFBs and the algorithm itself needs further attention.

There are very few publications addressing the PAPR reduction in the OFDM-OQAM scheme. Verification of the ideas and the simulation results is out of scope of this work. However, a brief review of some of these ideas is given here. For instance, a scheme called Overlapped Selected Mapping (OSLM) is proposed in [28; 27], where the conventional Selected Mapping technique is modified to account for the overlapping of the adjacent symbols. For $K = 4$, the PAPR reduction achieved by this method is reported to considerably less than that of the SLM technique for OFDM signal.

A modification of the PTS technique called Multi-Block Joint Optimization is presented in [23], where multiple blocks of QAM symbols are buffered. By dynamic programming, an optimum solution is proposed for obtaining the best phase

rotations. The simulation results reported suggest a PAPR reduction which is comparable or better than that achieved by the PTS technique for the OFDM signal. Another variation of the PTS technique is developed in [34], referred to as segmental PTS scheme which exploits the overlapping of the adjacent symbols to achieve remarkable PAPR reduction, at expense of some loss in the throughput.

5. INTERPOLATION

In this section, the LTE 5 MHz scenario is employed to investigate the possibility of interpolation for PAPR measurement. In many PAPR reduction methods, particularly those based on multiple signal representation, the algorithm needs to measure the PAPR of a candidate representation in each iteration. It is well-known that the critical sampling rate is not sufficient to capture the peaks of the OFDM signal in the time domain. As a rule of thumb, an oversampling of $L = 4$ is often used [31]. Oversampling implies a higher FFT size which leads to higher computational complexity.

In the considered scenario, the considerably high guard band provides the possibility of reducing the oversampling requirement by interpolation in the time domain. In the following sections, the idea is first introduced formally. Then a few filter designs are considered for the interpolation to investigate their performance in terms of detection error rate and computational complexity.

5.1 Subcarrier numbering

Throughout this text, the subcarrier numbering of the usual OFDM signal model of (2.13) is used, which is repeated here for convenience:

$$s[k] = \frac{1}{\sqrt{N}} \sum_{n=0}^{N-1} X_n e^{j\frac{2\pi}{N}nk}. \tag{5.1}$$

That is, the first subcarrier refers to zero-frequency and the last one refers to $(N-1)\frac{2\pi}{N}$.

Consider the frequency domain representation of the discrete-time signals, i.e., the Discrete-Time Fourier Transform (DTFT). It is well-known that the transform is 2π-periodic and the baseband portion of the spectrum corresponds to the $[-\pi, \pi]$ interval.

In the definition of (5.1), the index n counts the subcarriers from 0 to $N-1$ and assigns them to frequencies $0, \frac{2\pi}{N}, 2\frac{2\pi}{N}, \ldots, (N-1)\frac{2\pi}{N}$. This implies that the subcarriers $0, 1, \ldots, \frac{N}{2} - 1$ constitute the positive frequencies in $[0, \pi)$ and the subcarriers $\frac{N}{2}, \frac{N}{2} + 1, \ldots, N-1$ constitute the negative frequencies in $[-\pi, 0)$.

Following this numbering for the subcarriers, those reserved for the guard bands

must be located around the subcarrier $\frac{N}{2}$. Let N_g be an even number of null subcarriers. The subcarriers $\frac{N}{2}, \ldots, \frac{N}{2} + \frac{N_g}{2} - 1$ refer to the lower end of $[-\pi, \pi)$ and the subcarriers $\frac{N}{2} - \frac{N_g}{2}, \ldots, \frac{N}{2} - 1$ refer to the higher end of $[-\pi, \pi)$. This is illustrated in Figure 5.1a.

Considering the similarity of OFDM and OFDM/OQAM, the same considerations about the numbering of the subcarriers in the OFDM signal model holds for the OFDM/OQAM as well. To keep the explanations simple, the required methods and concepts are developed in the context of OFDM signal model.

5.2 Oversampling

In order to include oversampling in the OFDM signal generation, a larger FFT size must be used. The extra bins must be fed with null subcarriers located around the middle subcarriers; exactly similar to the case of guard bands. Figure 5.1b depicts the situation.

This could be simply illustrated as follows. Consider the sequence

$$x_1 = \{0, 1, 0, 1\}, \tag{5.2}$$

which refers to the input of an IDFT of length 4, i.e. $N = 4$. The four frequency bins correspond to $0, \frac{2\pi}{4}, 2\frac{2\pi}{4}, 3\frac{2\pi}{4}$. The 1's are chosen such that the IDFT sequence is real, that is

$$\begin{aligned} X_1[k] &= \sum_{n=0}^{3} x_{1n} e^{j\frac{2\pi}{4}nk} \\ &= e^{j\frac{2\pi}{4}k} + e^{j3\frac{2\pi}{4}k} = 2\cos(\frac{2\pi}{4}k). \end{aligned} \tag{5.3}$$

Adding 4 zeros around the center subcarrier, i.e. two times oversampling, yields a new sequence as

$$x_2 = \{0, 1, 0, 0, 0, 0, 0, 1\}, \tag{5.4}$$

which refers to the input of an IDFT of length 8, i.e. $N = 8$. The IDFT of this sequence will be

$$\begin{aligned} X_2[k] &= \sum_{n=0}^{7} x_{2n} e^{j\frac{2\pi}{8}nk} \\ &= 2\cos(\frac{2\pi}{8}k). \end{aligned} \tag{5.5}$$

To see the equivalence between $X_1[k]$ and $X_2[k]$, notice that $X_1[k]$ is defined over $k = 0, \ldots, 3$ and $X_2[k]$ is defined over $k = 0, \ldots, 7$. On the other hand, the discrete

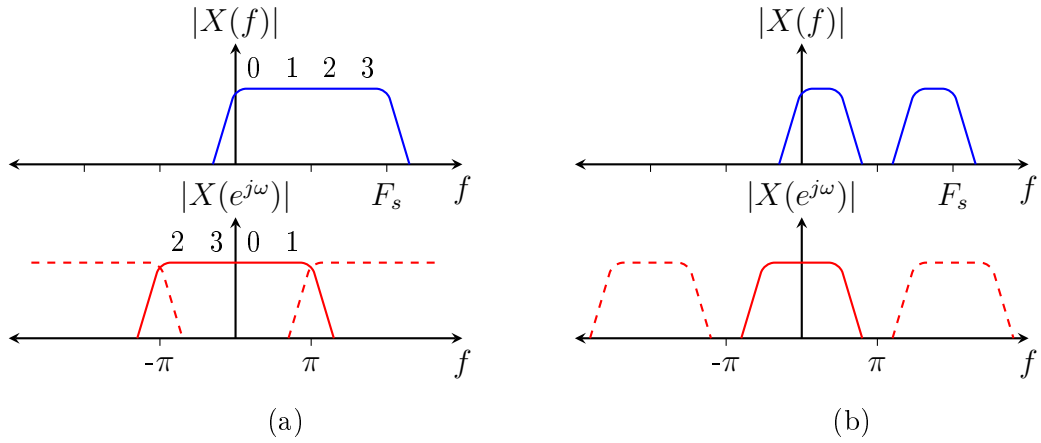

Figure 5.1: (a) Illustration of the role of subcarrier numbering in the PSD of the multicarrier signal. (b) the location of the guardband subcarriers

frequency of $X_2[k]$ is halved.

It is clear that padding zeros to the end of the sequence does not produce the desired signal. The IDFT would be, indeed, a sequence with higher number of points. However, it is completely a difference sequence since the zeros fill the whole negative half of the frequency band.

It is now clear that inserting guard bands is equivalent to the zero padding used for oversampling. In the considered scenario, 212 out of 512 subcarriers are null and reserved for guard bands. This suggests a readily available oversampling of about 2. We will first verify that the addition of the guard bands makes it possible to perform an oversampling of 2 and obtain the desired result. Then we will investigate the possibility of interpolation to perform the oversampling and discuss the gain in the computational complexity.

Figure 5.2a shows the CCDF curves of the basic OFDM scheme for the oversampling factors of $L = 1$, 2 and 4. The simulation results suggest negligible difference, even between $L = 1$ and $L = 4$. The situation, however, is completely different when the PAPR reduction methods are used. In other words, this small difference in the CCDF curves translates to a considerably large difference when the same setting for the PAPR measurement is used in an algorithm such as PTS. Figure 5.2b shows the CCDF curves when the PTS method is applied to the OFDM scheme. This shows that using a low oversampling factor causes considerable degradation in the performance of the algorithm. In addition, it confirms that an oversampling of $L = 2$ is sufficient, given that there is an inherent oversampling provided by the guard bands.

In conclusion, a second round of oversampling must be performed to reach $L = 4$ and obtain reliable CCDF curves. Since addition of guard bands causes empty

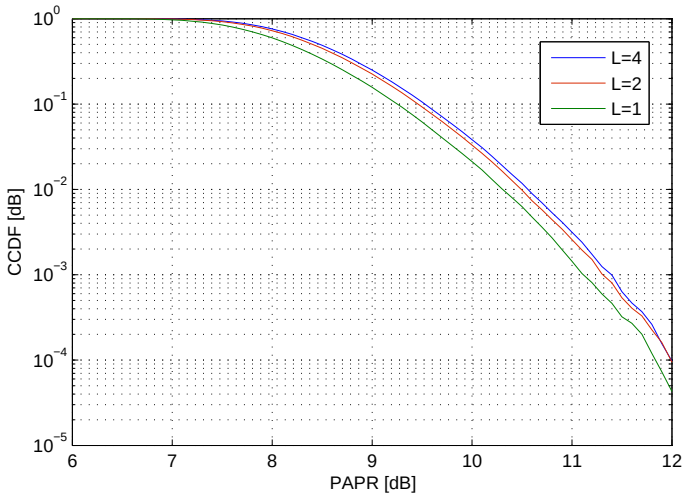

(a)

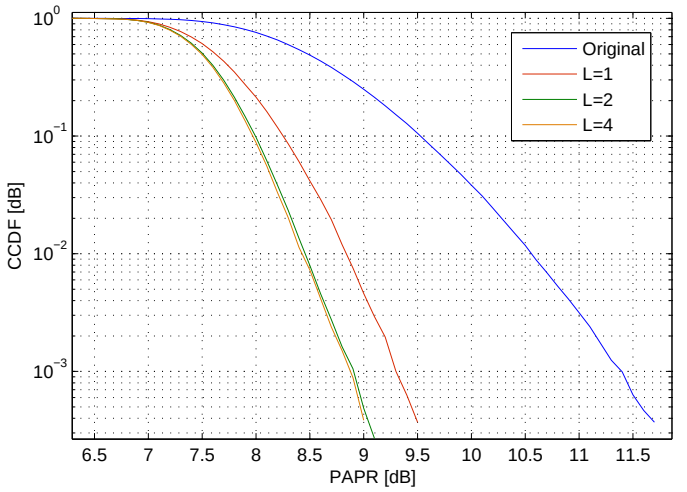

(b)

Figure 5.2: Effect of the guard bands on the oversampling requirement in the PAPR measurement, (a) on the basic OFDM signal and (b) on the PTS method.

spectrum in the high frequency part, it is possible to use interpolation to perform the second round of oversampling. In the next section, the interpolation problem is formally introduced and then its basic structure is discussed briefly.

It is worth mentioning that in the scenarios with rather small amount of guard bands, it is equivalently possible to perform oversampling by a factor of 2, and then use interpolation to reach the oversampling factor of 4. However, a gain in the computational complexity may be questionable.

5.3 Interpolation

In the normalized discrete-time frequency domain, the Fourier transform is 2π-periodic. Figure 5.3 illustrates how the frequency representation of a discrete-time

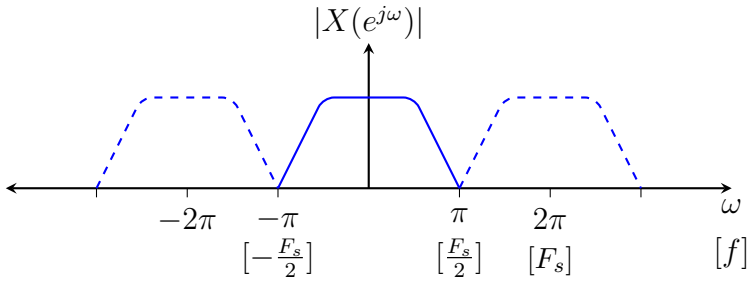

Figure 5.3: A schematic frequency representation in the normalized discrete-time frequency domain. Dashed lines are the replicas of the baseband portion.

signal looks like. It is common to refer to the $[-\pi, \pi]$ band as the baseband portion of the spectrum. Each period of the transform corresponds to an interval of length F_s, i.e., the sampling frequency. Therefore, the band $[0, 2\pi]$ corresponds to the interval $[0, F_s]$ in the unnormalized continuous-time frequency domain. Equivalently, the band $[-\pi, \pi]$ corresponds to $[-\frac{F_s}{2}, \frac{F_s}{2}]$.

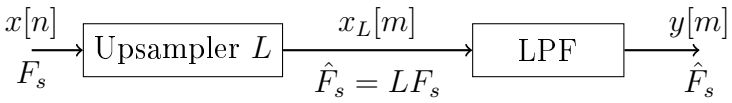

Figure 5.4: The basic structure of interpolation.

Figure 5.4 shows the basic structure of interpolation [14]. The discrete-time signal $x[n]$ is first upsampled by the desired factor, e.g. $L = 2$. The upsampled signal $x_2[m]$ has two times the initial sampling rate, i.e, $\hat{F}_s = 2F_s$. Upsampling is done by inserting $L-1$ zeros between adjacent samples. Figure 5.5 shows the effect of upsampling in the frequency domain; the sampling frequency is doubled while the frequency content remains intact. In other words, for the specific example of $L = 2$, a part of the adjacent replica enters the baseband portion. As shown in Figure 5.6, it is clear from the frequency domain representation that the interpolated signal can be obtained by filtering the extra content, i.e., to clean the spectrum from $\frac{F_s}{2}$ to $\frac{\hat{F}_s}{2}$.

It is clear that if the signal has significant energy over the entire range $[-\frac{F_s}{2}, \frac{F_s}{2}]$, namely the baseband portion, performing interpolation needs a very sharp filter. This is either impossible in practice or is computationally too expensive. The fully-loaded[1] critically-sampled OFDM signal is an example of a signal that has no room near the upper frequency part for a feasible interpolation filtering. This is why the guard bands could make it feasible to perform the interpolation.

[1]The term "fully-loaded" OFDM signal, refers to the case where all the subcarriers are active, i.e., all of them are modulated with data symbols.

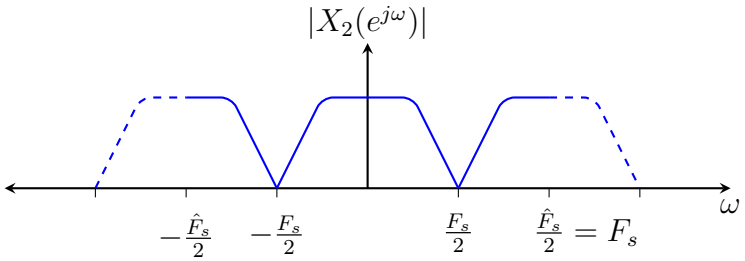

Figure 5.5: The upsampled version of the signal in Figure 5.3. The new sampling frequency is doubled $\hat{F}_s = 2F_s$. Dashed lines are the replicas of the expanded baseband portion.

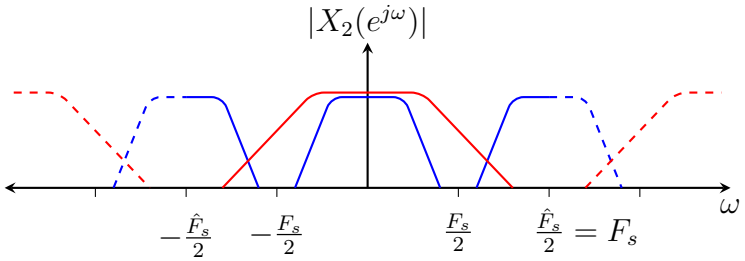

Figure 5.6: The situation of Figure 5.5 depicted for a signal that does not occupy the whole spectrum. The red lines refer to the interpolation filter.

5.4 Linear-phase FIR filters

Here the characteristics of the FIR filters are briefly presented. The purpose of this quick review is to introduce the terminology used in the subsequent sections. Figure 5.7 illustrates the general frequency response of a lowpass FIR filter. The response consists of three bands; the passband $[0, \omega_p]$ where maximum deviation from unity must be δ_p, transition band $[\omega_p, \omega_s]$, and stopband $[\omega_s, \pi]$ where the minimum attenuation must be δ_s.

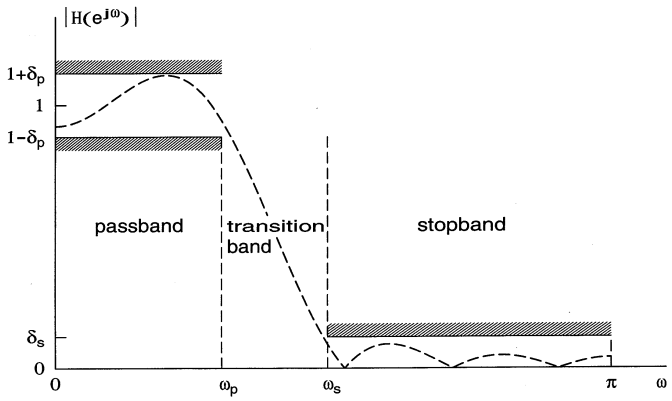

Figure 5.7: A generic frequency response of an FIR filter.

The amplitude characteristics are represented by the maximum passband variation A_p defined as

$$A_p = 20 \log_{10} \left(\frac{1 + \delta_p}{1 - \delta_p} \right) \quad \text{dB}, \tag{5.6}$$

and the minimum stopband attenuation A_s as

$$A_s = -20 \log_{10} \delta_s \quad \text{dB}. \tag{5.7}$$

The complexity of an FIR filter depends on its order, i.e., the number of its taps. The sharpness of the transition band, as well as the amplitude requirements, determine the complexity of the filter. In other words, the filter order increases in one or more of these cases: higher sharpness or lower $\Delta\omega = \omega_s - \omega_p$, less deviation in the passband or lower δ_p, and more attenuation in the stopband or higher δ_s.

It is required that the signal content that falls into the passband of the filter is preserved both in amplitude and in phase. Therefore, the phase response of the filter must be linear in the passband. The FIR filters employed in this work are called linear-phase FIR filters designed by the Parks-McClellan algorithm which is readily available via the `firpm` function in MATLAB. In the sequel, as will be explained shortly, even-order filters are only considered. In addition, it is desired to have real filter coefficients.

The computational complexity of an FIR filter is expressed by the number of real additions and real multiplications for generation of one output sample. For simplicity, and since multiplication is much more demanding than addition, only the number of multiplications is considered. Linear-phase FIR filters have symmetry in the coefficients, which can be exploited to reduce the number of multipliers. Therefore, for a filter of order M, $\frac{M}{2} + 1$ complex multiplications per output sample are needed. Given that the coefficients are real-valued and the signal is complex-valued, it is equal to $M + 2$ real multiplications per output sample.

In the case of interpolation, the input signal is upsampled, i.e. there are regular zero samples, which do not contribute to the output value. Therefore, it can be shown that the upsampling can be done after the multipliers, avoiding the multiplications by zero. Finally, exploiting the coefficient symmetry of the linear-phase FIR filters, an efficient filtering with $\frac{M+2}{L}$ real multiplications per output sample is feasible.

In the OFDM transmitter, the so-called block processing is done, i.e., each symbol is processed separately. The FFT processing is a major source of computational complexity, which is expressed by the number of multiplications required for generating a set of outputs. Therefore, the number of multiplications per output sample is not informative enough about the complexity of the filter. In this report, the computational complexity is expressed by the number of operations required for

Order	$N = 128$	$N = 512$
2	33 %	50 %
4	0 %	25 %
6	-33 %	0 %

Table 5.1: The reduction in complexity for an oversampling factor of $L = 2$, obtained by using FIR filters for interpolation, compared to the direct oversampling by larger FFT size.

generating a whole OFDM symbol.

In this application, for an OFDM symbol with N subcarriers, i.e., N FFT bins, the upsampled signal has $2N$ samples, on which the FIR filtering is performed. Therefore, $2N(\frac{M}{2}+1)$ real multiplications are required to perform the interpolation on each OFDM symbol. The number of the real multiplications for an N-point IDFT implemented by the FFT Split-Radix algorithm is $N(\log_2 N - 3) + 4$ [2]. If the oversampling is provided by doubling the size of the FFT block, consider the additional required multiplications comparing to those of an N-point block. For quick reference, the complexity reduction for different filter orders are listed in Table 5.1. Clearly, the benefit of using interpolation by FIR filters instead of direct oversampling becomes more substantial as the number of subcarriers increases.

5.5 Finite-length sequences and filtering

Filtering a signal stems from the need to modify its spectrum based on a specific mask, namely the frequency response of the filter. This is intended to be done by multiplication of the frequency response and the spectrum of the signal. In the context of finite-length sequences, such as OFDM symbol, this operation is done by circular convolution [20, Chapter 8]. As a brief explanation, a finite-length discrete-time sequence is represented in the frequency domain using the Discrete Fourier Transform (DFT.) This transformation is based on assuming a periodic signal built from the finite-length sequence. Linear convolution of this periodic signal is completely meaningful and gives the desired modification in the frequency domain. It is easy to see that linear convolution of a periodic signal is equivalent to circular convolution of one period of it. Therefore, in the filtering operation required for interpolation, it is necessary to perform the circular convolution.

However, the filtering is inherently done in the linear way. In other words, the circular convolution must be imitated, which is equivalent to linear filtering on the periodic signal build from the finite-length signal. This can be done by copying a segment from the end of the finite-length sequence to its beginning, building the relevant part of the underlying periodic signal. This segment is called the Cyclic Prefix (CP) and its length must be equal or greater than the filter order, i.e., the number

of the past samples that the filter needs at the beginning of the sequence. After performing the linear convolution on this new sequence, the CP is discarded from the beginning and the remaining sequence is the result of the circular convolution.

It must be mentioned that the aforementioned Cyclic Prefix is different from the one used in the OFDM scheme to prevent from the distortion due to the frequency-selective channel, though both are based on the same concept. The latter is referred to as the channel CP in this section. As a matter of fact, the channel CP is added to the OFDM symbol in a later stage. Therefore, in the discussion of the interpolation on the OFDM signal, the channel CP is not a part of the signal.

In addition, note that the main ideas are developed based on the non-causal filter which has symmetric impulse response and, hence, zero phase response. However, in practice the filter must be causal, i.e. the impulse response is shifted and the filter becomes linear-phase. In the application of causal linear-phase FIR filters, it is always necessary to take the delay, or equivalently the phase term in the frequency domain, into account. The delay in the case of finite-length sequences can be discarded by circular shift of the filtered symbol. It is easy to see that the delay in this class of filters is equal to $\frac{M}{2}$ samples.

The odd-order linear-phase FIR filters cause a delay of $M/2$ samples, which is a non-integer value. Eliminating the sub-sample delay needs higher complexity. Therefore, in this work only the even-order FIR filters are considered.

In the case of the OFDM/OQAM signal, the concept of block processing is no more relevant, as the symbols are interleaved in the time domain. In other words, the signal, as in its basic form, should be viewed as an infinite-length seamless signal. It is possibly necessary to apply the FIR filter to the signal in a segment-by-segment manner. In this case, the memory elements of the filter must not be reset.

5.6 Case Study - OFDM, LTE 5 MHz

In the case of the 5 MHz configuration of the LTE standard, in addition to one nulled DC subcarrier, there are 211 subcarriers reserved for the guard bands out of 512 subcarriers. It was discussed that this provides roughly an oversampling of two. Thus interpolation by a factor of two yields the resolution required for the PAPR measurement. The PSD of the OFDM signal in this scenario is shown in Figure 5.8. As expected, there is about 40% of weak spectrum content in the higher frequency band. Note that the PSD of the OFDM signal is slightly different if the channel CP is added to the signal. However, as discussed before, the channel CP is added in a later stage of the transmitter.

The upsampled signal is shown in Figure 5.9a. The passband and stopband frequencies can be roughly determined by inspecting Figure 5.9b. The part of the spectrum which must be preserved covers up to nearly 0.3π rad/sec. The transition

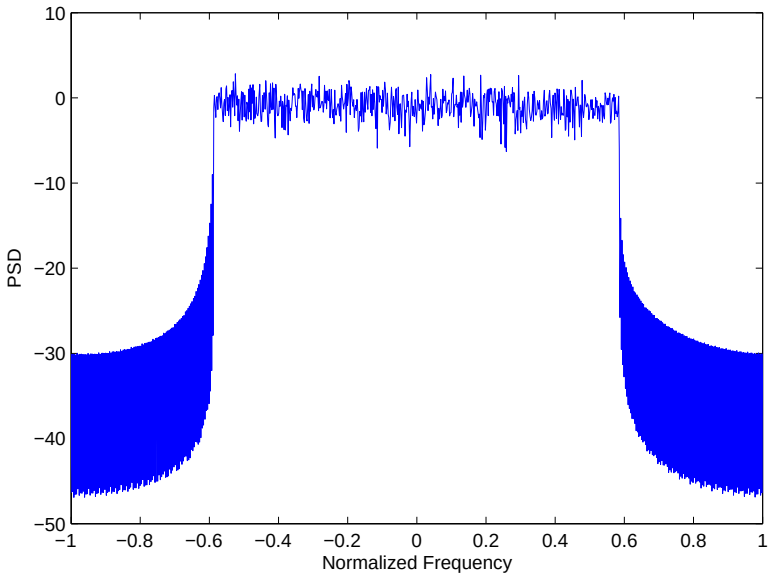

Figure 5.8: The PSD of the OFDM signal in the LTE 5 MHz scenario, which has 212 null and 300 active subcarriers.

band of the filter does not need to be very sharp as the signal content is weak in the range of 0.3π to 0.7π rad/sec. First, an FIR filter with the choice of parameters which leads to nearly perfect performance is applied to the signal and the results are detailed. Next, several designs for the FIR filters are done and the results are presented briefly. The objective is to find the best FIR filter in terms of the computational complexity and performance. A trade-off is obviously expected.

A sharp filter

We will first consider a very sharp filter with $\omega_p = 0.5$ and $\omega_s = 0.55$ and with strict attenuations $\delta_p = 0.001$ and $\delta_s = 0.001$. Such a filter needs an order of $M = 132$ and is certainly not interesting for practical purposes. However, the purpose of this discussion is to verify the validity of the interpolation idea for the PAPR measurement. The frequency response of the filter is shown in Figure 5.10.

Figure 5.11 shows the PSD of the interpolated signal against the original one, which match closely. The case of ideal channel is simulated for 16QAM modulation. The SER curve for this scenario closely matches that of a basic OFDM scheme for typical constellation dimensions. The time-domain behavior can be illustrated by observing the negligible error power between the interpolated signal and the directly oversampled one, as shown in Figure 5.12. Finally, it is clear that the PAPR characteristics of the interpolated waveform is nearly identical to that of the directly oversampled one.

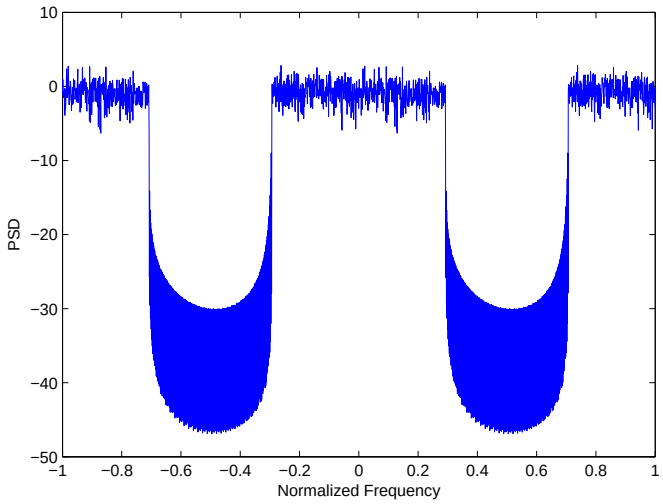

(a)

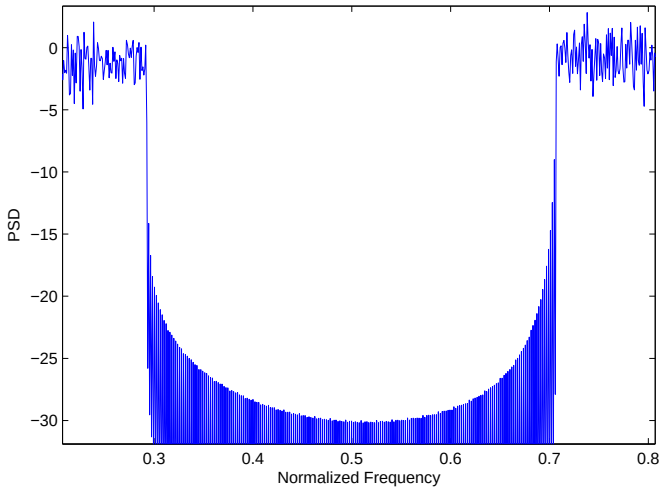

(b)

Figure 5.9: The PSD of the upsampled OFDM signal in the LTE 5 MHz scenario. (a) the whole band, (b) zoomed in to show the details needed for choice of the filter characteristics.

FIR Order 4

The above observation, based on a very sharp filter, verifies the idea of the interpolation. Next, we will investigate the performance of a 4^{th}-order FIR filter with these characteristics: maximum deviation from unity of 3.3 dB in $[0, 0.3\pi]$ and minimum attenuation of 15.2 dB in $[0.7\pi, \pi]$. The frequency response of the filter is shown in Figure 5.13.

The distorted constellation of the interpolated signal, based on the filter of Figure 5.13, is shown in Figure 5.14a. The detected symbols are stretched along the radial lines. In other words, the phase of the symbols are remained unchanged, but the amplitude is distorted. This is, indeed, expected as a linear-phase FIR filter is

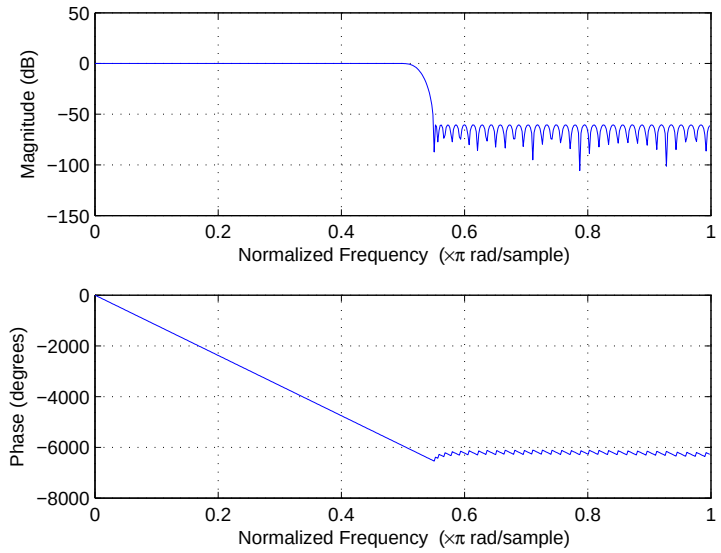

Figure 5.10: Frequency response of a lowpass FIR filter of order $M = 132$ for $\omega_p = 0.5$, $\omega_s = 0.55$, $\delta_p = 0.001$ $\delta_s = 0.001$.

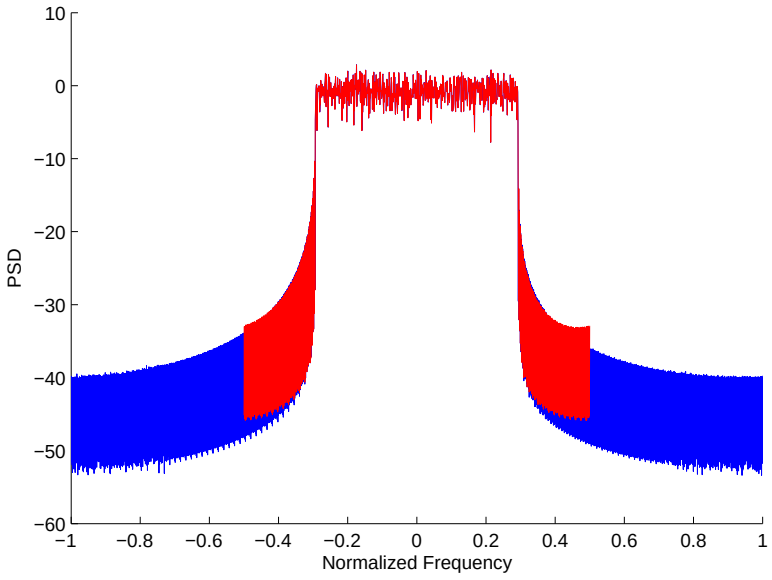

Figure 5.11: The PSD of the interpolated signal, the blue curve, compared to the original one. The interpolation filter of Figure 5.10 is used.

used. The distortion in the amplitude is due to the poor characteristics of the filter in the passband, which leads to the SER curve of Figure 5.14b.

The PSD of the interpolated signal is shown in Figure 5.15, where seemingly slight distortion in the passband and rather strong content in the high frequencies are observed. It will be shown that the undesired components of this magnitude in the high frequency range will not cause considerable performance loss. On the

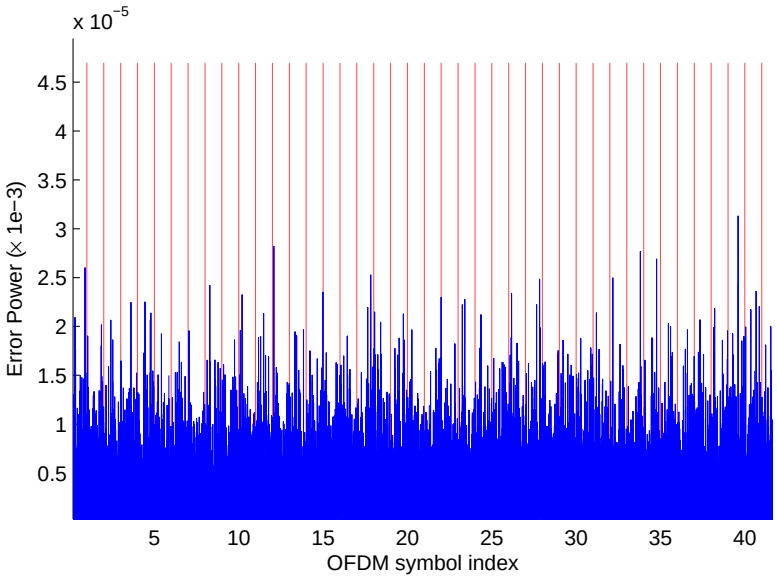

Figure 5.12: The error power between the interpolated signal and the directly oversampled one. The red lines distinguish the OFDM symbols.

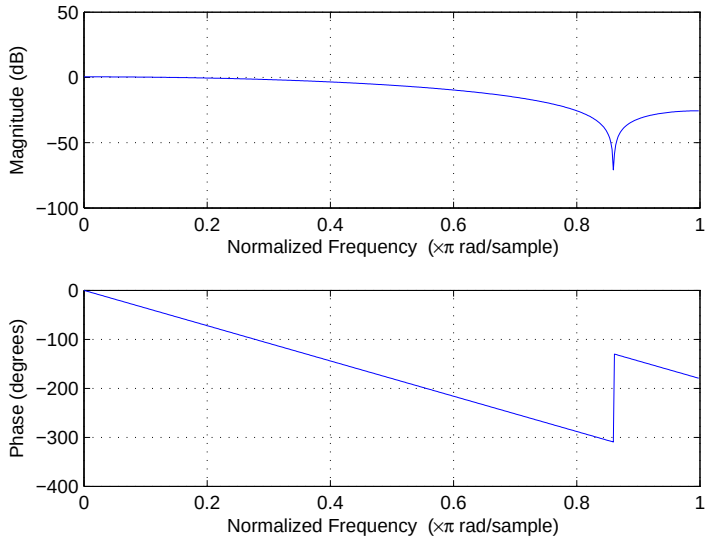

Figure 5.13: Frequency response of a lowepass FIR filter of order $M = 4$. Maximum deviation from unity in $[0, 0.3\pi]$: 3.3 dB, Minimum attenuation in $[0.7\pi, \pi]$: 15.2 dB.

other hand, the filter characteristic is much more important in the passband. The interpolation is repeated by a similar 4^{th}-order filter which has a maximum deviation from unity of 1 dB in $[0, 0.3\pi]$ and minimum attenuation of 10 dB in $[0.7\pi, \pi]$. That is, better characteristics in the passband but worse in the stopband. The distorted constellation and the SER curve are shown in Figure 5.16a and Figure 5.16b. The performance is clearly improved, confirming the stated observation.

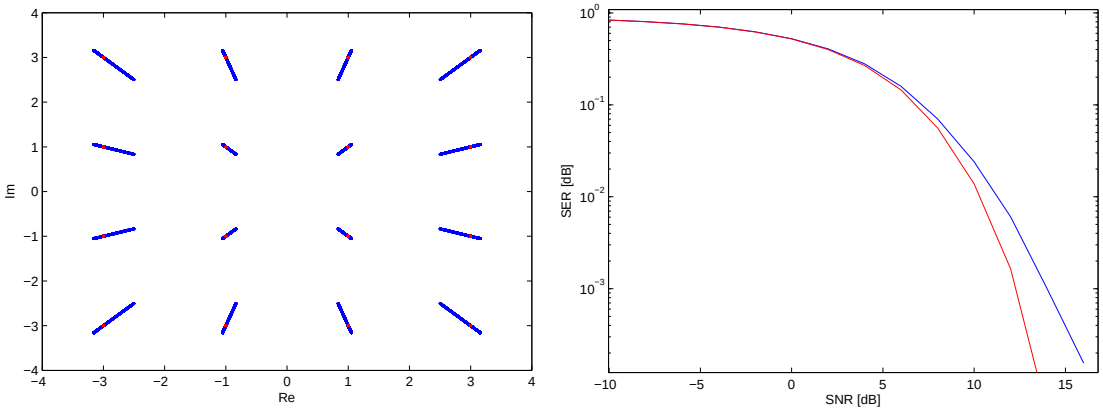

(a) (b)

Figure 5.14: (a) Distorted constellation and (b) SER of the interpolated OFDM signal after detection, the blue curve, using the filter of Figure 5.13.

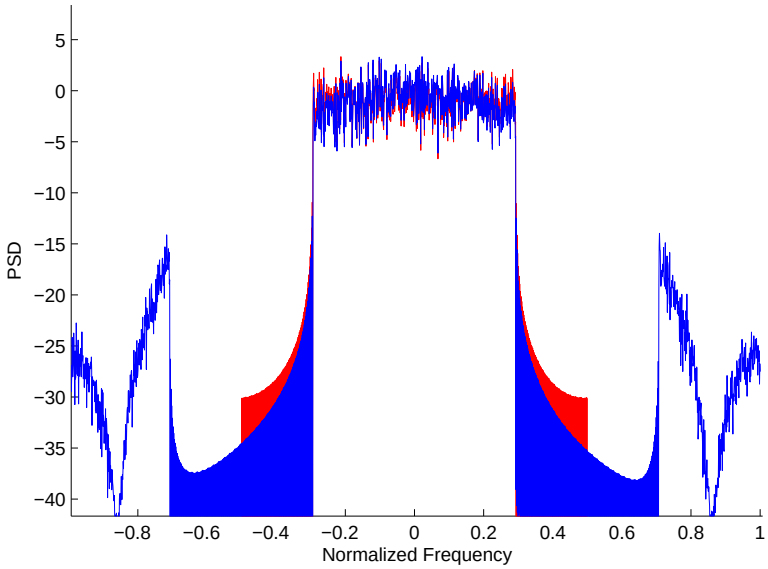

Figure 5.15: The PSD of the interpolated signal, the blue curve, compared to the original one. The interpolation filter of Figure 5.13 is used.

FIR Order 2

Finally, the performance of an FIR filter of order 2 is investigated on this scenario. As there is only one degree of freedom in the order-2 linear-phase FIR filters, the design is done manually. Such a filter, with real coefficients, has a pair of complex conjugate zeros which must lie on the unit circle. The phase of the zeros determine the notch location in the frequency domain. It can be easily seen by trial and error that the only way to get reasonable passband and stopband characteristics is to put the zeros on the second half of the band, i.e., in $[\frac{\pi}{2}, \pi]$.

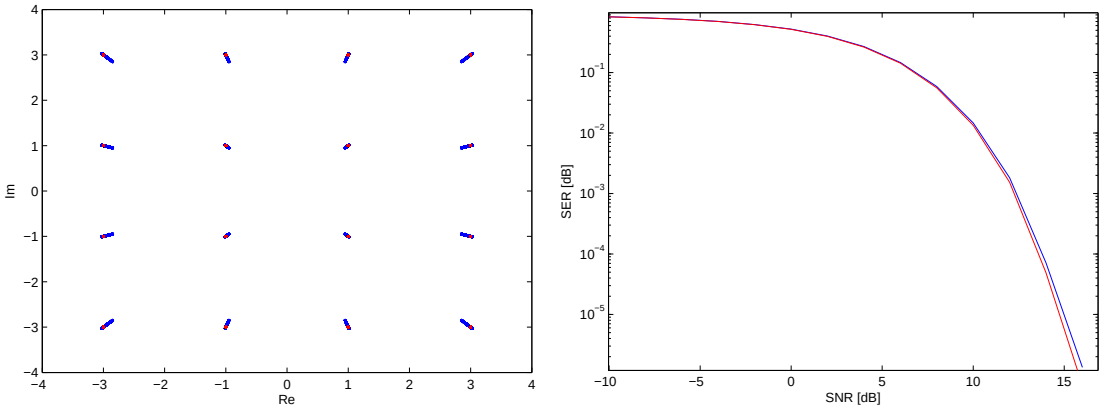

(a) (b)

Figure 5.16: (a) Distorted constellation and (b) SER of the interpolated OFDM signal after detection, using a 4^{th}-order filter, maximum deviation from unity of 1 dB in $[0, 0.3\pi]$ and minimum attenuation of 10 dB in $[0.7\pi, \pi]$.

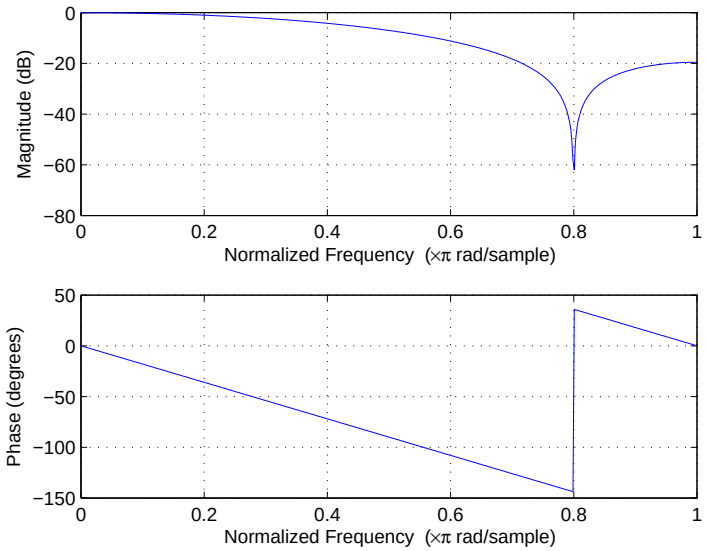

Figure 5.17: Frequency response of a lowpass FIR filter of order $M = 2$ with its notch(zeros) at $\omega = 0.8\pi$. Maximum deviation from unity in $[0, 0.3\pi]$: 4.46 dB, Minimum attenuation in $[0.7\pi, \pi]$: 18.37 dB.

The interpolation is done using an order-2 filter with its notch located at $\omega = 0.8\pi$. The frequency response, distorted constellation and the SER curve are shown in Figure 5.17, Figure 5.18a, Figure 5.18b, respectively. As expected, the distortion is considerably higher than the case of 4^{th}-order FIR filter. As explained before, this is mostly due to the poor passband behavior of the filter.

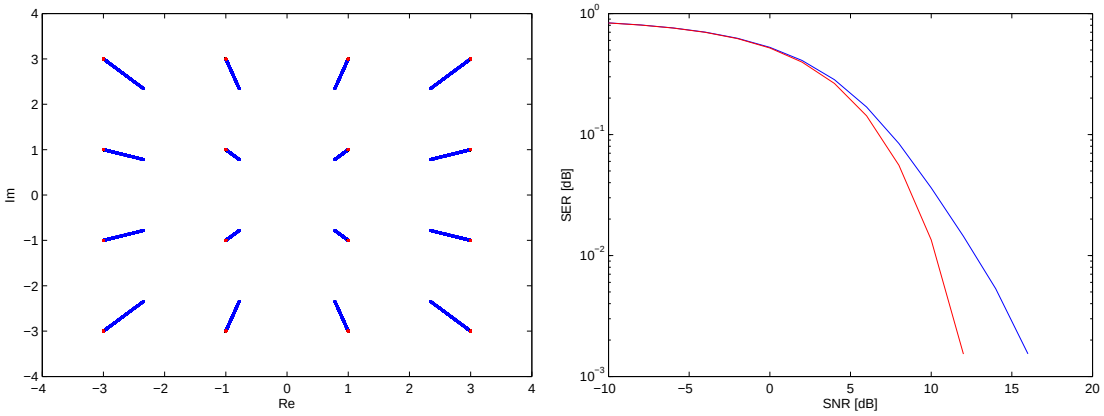

(a) (b)

Figure 5.18: (a) Distorted constellation and (b) SER of the interpolated OFDM signal after detection, the blue curve, using the 2^{nd}-order filter of Figure 5.17.

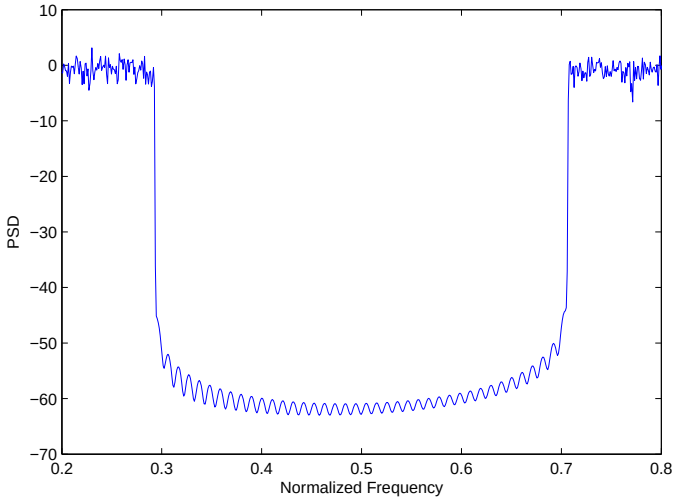

Figure 5.19: The PSD of the upsampled OFDM/OQAM signal in the LTE 5 MHz scenario; zoomed in to show the details needed for the choice of the filter characteristics.

5.7 Case Study - OFDM/OQAM, LTE 5 MHz

The PSD of the upsampled OFDM/OQAM signal based on the LTE 5 MHz scenario is shown in Figure 5.19, which is zoomed into the interval where the transition band of the interpolation filter should be located. The clear and expected difference between the OFDM and OFDM/OQAM signals is that the latter is very well-localized in the frequency domain. That is, the band around $\omega = 0.5\pi$ does not contain considerable signal content. This can be observed by applying a sharp interpolation filter with, e.g., $\omega_c = 0.4\pi$ to both signals. It can be shown by simulations that the distortion in the case of the OFDM signal is considerable, while it is negligible in the

case of the OFDM/OQAM signal. Although this observation does not directly contribute to the filter design, it could provide insight into the structure of the signals in question.

The OFDM/OQAM signal exhibits similar behavior to that of the OFDM signal under interpolation using linear-phase FIR filters. The OFDM/OQAM signal model is much more complicated than the OFDM signal model. However, the intricacy lies in the special phase arrangement of the adjacent symbols in both the time and the frequency domains. Since the linear-phase FIR filter does not distort the phase characteristics of the signal, it behaves in an almost identical way to the OFDM signal. Therefore, it is immaterial to present the simulation results of the interpolation for the OFDM/OQAM signal.

6. CONCLUSION

An in-depth review of the OFDM and OFDM/OQAM signal models is presented in Chapter 2. It starts from the very general structure of multipulse modulation and the generalized Nyquist criterion. Then the challenge in changing the rectangular pulse shape of the OFDM is discussed. It is well-known that the OFDM has high spectral side lobes and adopting well-localized pulse shapes is necessary for the emerging applications. The chapter continues with the original idea behind the CMT scheme, followed by the SMT scheme. And finally the discrete-time model of the OFDM/OQAM is briefly presented. The objective of this chapter is to make the structure of this scheme, particularly the purpose of OQAM pre- and post-processing, clear to the reader. A good knowledge of this scheme is necessary for adaptation of the previously proposed PAPR reduction methods for OFDM.

The PAPR problem and the statistical characteristics of the OFDM and OFDM-OQAM signal model were discussed in Chapter 3. It was concluded that the CCDF of the PAPR is the same for both schemes, given that the orthogonality is met in the pulse shapes of the latter. The chapter was finalized by introducing some of the PAPR reduction methods.

The adaptation of the SLM and PTS techniques to the OFDM/OQAM signal model was discussed in Chapter 4. Through a simplistic example, the challenges were investigated. It was explained that the overlapping of the adjacent symbols limits the optimization capability. Although acceptable PAPR reduction was shown to be possible by the PTS method, the computational complexity is a major concern. There are very few publications available on this issue and there is room for considerable contributions to the field.

In some scenarios, the guard band is wide enough to provide an oversampling of nearly two. The remaining resolution could be achieved by either an oversampling of 2, or via an interpolation by 2. There is a likely gain in the computational complexity if interpolation is used instead of oversampling. This idea was explored in Chapter 5. It was shown that the gain of this technique depends on how strictly the filtering stage of the interpolation must be done. For the investigated scenario of LTE 5 MHz, an FIR filter of order 4 results in good performance. This scheme would yield a reduction of 25% in the complexity. Small but not negligible, there is degradation in the SER as a consequence of applying more relaxed filters. As a

further research direction, pre-distortion of the data symbols is possible, such that the effect of the filters on the system performance is eliminated.

Finally, the research area of PAPR reduction is seemingly experiencing a new era of fresh activity. The necessity stems from the urge to use the modern multicarrier waveforms in the advanced physical layers of the next generations of wireless systems.

BIBLIOGRAPHY

[1] Emre Telat Ar and I. Emre Telatar. Capacity of multi-antenna gaussian channels. *European Transactions on Telecommunications*, 10:585–595, 1999.

[2] L.G. Baltar, F. Schaich, M. Renfors, and J.A. Nossek. Computational complexity analysis of advanced physical layers based on multicarrier modulation. In *Future Network Mobile Summit (FutureNetw), 2011*, pages 1–8, June 2011.

[3] R.W. Bauml, R. F H Fischer, and J.B. Huber. Reducing the peak-to-average power ratio of multicarrier modulation by selected mapping. *Electronics Letters*, 32(22):2056–2057, Oct 1996.

[4] M. Breiling, S.H. Muller-Weinfurtner, and J.B. Huber. SLM peak-power reduction without explicit side information. *Communications Letters, IEEE*, 5(6):239–241, June 2001.

[5] Robert W. Chang. Synthesis of band-limited orthogonal signals for multichannel data transmission. *Bell Sys. Tech. J.*, pages 1775–1796, December 1966.

[6] H. Chen and A.M. Haimovich. Iterative estimation and cancellation of clipping noise for OFDM signals. *Communications Letters, IEEE*, 7(7):305–307, July 2003.

[7] L.J. Cimini and N.R. Sollenberger. Peak-to-average power ratio reduction of an OFDM signal using partial transmit sequences. *Communications Letters, IEEE*, 4(3):86–88, March 2000.

[8] B. Farhang-Boroujeny. OFDM versus filter bank multicarrier. *Signal Processing Magazine, IEEE*, 28(3):92–112, May 2011.

[9] Behrouz Farhang-Boroujeny and Chung Him Yuen. Cosine modulated and offset QAM filter bank multicarrier techniques: a continuous-time prospect. *EURASIP J. Adv. Signal Process*, 2010:6:1–6:11, January 2010.

[10] D. Guel and Jacques Palicot. Analysis and comparison of clipping techniques for OFDM peak-to-average power ratio reduction. In *Digital Signal Processing, 2009 16th International Conference on*, pages 1–6, July 2009.

[11] Seung Hee Han and Jae Hong Lee. An overview of peak-to-average power ratio reduction techniques for multicarrier transmission. *Wireless Communications, IEEE*, 12(2):56–65, April 2005.

[12] Dukhyun Kim and G.L. Stuber. Clipping noise mitigation for OFDM by decision-aided reconstruction. *Communications Letters, IEEE*, 3(1):4–6, Jan 1999.

[13] Edward A. Lee and David G. Messerschmitt. *Digital communications*. Kluwer academic publishers, second edition, 1994.

[14] Sanjit K. Mitra and James F. Kaiser, editors. *Handbook for Digital Signal Processing*. John Wiley & Sons, Inc., New York, NY, USA, 1st edition, 1993.

[15] S.H. Muller and J.B. Huber. OFDM with reduced peak-to-average power ratio by optimum combination of partial transmit sequences. *Electronics Letters*, 33(5):368–369, Feb 1997.

[16] Richard van Nee and Ramjee Prasad. *OFDM for Wireless Multimedia Communications*. Artech House, Inc., Norwood, MA, USA, 1st edition, 2000.

[17] H. Ochiai and H. Imai. Performance of the deliberate clipping with adaptive symbol selection for strictly band-limited OFDM systems. *Selected Areas in Communications, IEEE Journal on*, 18(11):2270–2277, Nov 2000.

[18] N. Ohkubo and T. Ohtsuki. Design criteria for phase sequences in selected mapping. In *Vehicular Technology Conference, 2003. VTC 2003-Spring. The 57th IEEE Semiannual*, volume 1, pages 373–377 vol.1, April 2003.

[19] R. O'Neill and L.B. Lopes. Envelope variations and spectral splatter in clipped multicarrier signals. In *Personal, Indoor and Mobile Radio Communications, 1995. PIMRC'95. Wireless: Merging onto the Information Superhighway., Sixth IEEE International Symposium on*, volume 1, pages 71–75 vol.1, Sep 1995.

[20] Alan V. Oppenheim, Ronald W. Schafer, and John R. Buck. *Discrete-time Signal Processing (2nd Ed.)*. Prentice-Hall, Inc., Upper Saddle River, NJ, USA, 1999.

[21] Athanasios Papoulis. *Probability, Random Variables, and Stochastic Processes*. McGraw-Hill, second edition, 1984.

[22] Man-on Pun, Michele Morelli, and C. C. Jay Kuo. *Multi-Carrier Techniques For Broadband Wireless Communications: A Signal Processing Perspectives*. Imperial College Press, London, UK, UK, 2007.

[23] Daiming Qu, Shixian Lu, and Tao Jiang. Multi-block joint optimization for the peak-to-average power ratio reduction of FBMC-OQAM signals. *Signal Processing, IEEE Transactions on*, 61(7):1605–1613, April 2013.

[24] M. Renfors, F. Bader, L. Baltar, D. Le Ruyet, D. Roviras, P. Mege, M. Haardt, and T. Hidalgo Stitz. On the use of filter bank based multicarrier modulation for professional mobile radio. In *Vehicular Technology Conference (VTC Spring), 2013 IEEE 77th*, pages 1–5, June 2013.

[25] H. Saeedi, M. Sharif, and F. Marvasti. Clipping noise cancellation in OFDM systems using oversampled signal reconstruction. *Communications Letters, IEEE*, 6(2):73–75, Feb 2002.

[26] P. Siohan, C. Siclet, and N. Lacaille. Analysis and design of OFDM/OQAM systems based on filterbank theory. *Signal Processing, IEEE Transactions on*, 50(5):1170–1183, May 2002.

[27] A. Skrzypczak, J.-P. Javaudin, and P. Siohan. Overlapped selective mapping for pulse-shaped multi-carrier modulations. In *Vehicular Technology Conference, 2006. VTC-2006 Fall. 2006 IEEE 64th*, pages 1–5, Sept 2006.

[28] A. Skrzypczak, J.-P. Javaudin, and P. Siohan. Reduction of the peak-to-average power ratio for the OFDM/OQAM modulation. In *Vehicular Technology Conference, 2006. VTC 2006-Spring. IEEE 63rd*, volume 4, pages 2018–2022, May 2006.

[29] A. Skrzypczak, P. Siohan, and J.-P. Javaudin. Analysis of the peak-to-average power ratio for OFDM/OQAM. In *Signal Processing Advances in Wireless Communications, 2006. SPAWC '06. IEEE 7th Workshop on*, pages 1–5, July 2006.

[30] Jose Tellado. *Multicarrier Modulation with Low PAR: Applications to DSL and Wireless*. Kluwer Academic Publishers, Norwell, MA, USA, 2000.

[31] C. Tellambura. Computation of the continuous-time PAR of an OFDM signal with BPSK subcarriers. *Communications Letters, IEEE*, 5(5):185–187, May 2001.

[32] P. P. Vaidyanathan. *Multirate Systems and Filter Banks*. Prentice-Hall, Inc., Upper Saddle River, NJ, USA, 1993.

[33] Ari Viholainen, Maurice Bellanger, and Mathieu Huchard. PHYDYAS project, deliverable 5.1: Prototype filter and structure optimization. Technical report, FP7-ICT, January 2009.

[34] Chen Ye, Zijun Li, Tao Jiang, Chunxing Ni, and Qi Qi. Papr reduction of OQAM-OFDM signals using segmental PTS scheme with low complexity. *Broadcasting, IEEE Transactions on*, 60(1):141–147, March 2014.

[35] G.T. Zhou and Liang Peng. Optimality condition for selected mapping in OFDM. *Signal Processing, IEEE Transactions on*, 54(8):3159–3165, Aug 2006.